TESINA D'ESPECIALITAT

Títol

An analysis of the design and assembly of the AAR tri-axial machine

Autor/a

Jonathan Stokes

Tutor/a

Ignacio Carol y Carlos Maria Lopez

Departament

Enginyeria de Camins, Canals i Ports

Intensificació

Estudio de morteros y hormigones bajo ataque álcali-árido

Data

Junio 2011

Acknowledgements

I would firstly like to thank Joaquín Liaudat, who worked alongside me this year and without whose help this thesis would not have reached the point it has today.

I would like to thank my tutors Ignacio Carol and Carlos Maria Lopez for their patience and for finding time to give me guidance for this thesis.

To my girlfriend Anna-Joy for her love, support, encouragement and occasional disbelief at the complexity of concrete.

I would like to thank Elizabeth Stokes, for her invaluable help with proof reading and the final preparation of this document.

Finally, thank you to my flatmates Adriana Briseño for the loud motivational Mexican music when times were hard, Oliver Teall who worked at the table next to me on his thesis and kept me motivated, and Jos van der Boom for his good humour.

Abstract

Title An analysis of the design and assembly of the AAR tri-axial machine.

Author Jonathan Stokes

Tutor Ignacio Carol y Carlos Maria Lopez

The following work is an analysis of the design and reassembly of a tri-axial machine in the laboratory at UPC designed to test the expansive alkali-silica reactions that can occur in concrete under various conditions.

The expansive reactions between alkalis and alkali-reactive aggregates within concrete structures are a problem which has been known about since the mid 20th century. This slow-evolving concrete damage causes a huge amount of damage to susceptible concrete structures worldwide. This damage is serious because it leads to a degradation of the material properties of the concrete, leading to a less safe structure. This phenomenon is the leading cause of dam concrete deterioration.

Much research has been carried out in this field in attempting to understand the causes; however the engineering community is far from fully understanding and being able to predict expansions caused by this reaction as it can vary greatly with environmental conditions. This thesis presents a summary of the main factors which affect this reaction, which are the temperature, humidity and confinement stresses. This is given with a view to explaining the design of the experimental testing machine.

The aim of the experimental results the machine will provide is to further refine and understand the processes behind the alkali-silica expansion, which will help in the refinement of current expansion-prediction models and in the creation of new models. A brief analysis of some of the main expansion prediction models is given as background to the design of the machine.

The main body of work carried out this year has been the assembly of the experimental machine, with all of the work required to set up a one of a kind machine such as this in a new environment. The final parts of this thesis provide detailed information on the workings and setup of each of the systems the machine relies on for the benefit of the next users, as well as information on its current status and a guide to future operation.

Keywords: alkali-aggregate reaction, alkali-silica reaction, modelling, experimental testing

Resumen

Titulo Un estudio sobre el diseño y la construcción del equipo de ensayos tri-axial sobre RAA

Autor Jonathan Stokes

Tutores Ignacio Carol y Carlos Maria Lopez

El trabajo a continuación es un análisis del diseño y reconstrucción de una maquina tri-axial en el laboratorio de la UPC diseñado para comprobar la expansión a causa de reacciones alcali-silice que pueden ocurrir en el hormigón.

Estas reacciones expansivas entre álcalis y áridos álcali-reactivos dentro de las estructuras de hormigón son una patología de algunos hormigones conocido desde el medio del siglo 20. Este proceso se evoluciona lentamente causando una enorme cantidad de daño cada año a estructuras de hormigón sensibles a esta reacción. Este daño es muy serio porque resulta en una degradación de las propiedades mecánicas del hormigón, dejando una estructura menos seguro. Este fenómeno es la principal causa de deterioración de presas de hormigón.

Muchas investigaciones han sido elaboradas en este ámbito intentando entender las causas, pero todavía se está lejos de de poder predecir con certeza su parición, y evaluar cuantitativamente su magnitud debido a la gran variación del proceso debido a diferentes condiciones ambientales. Esta tesina presenta un resumen de los factores principales que afectan a esta reacción, que son la temperatura, la humedad y el confinamiento. Este resumen esta presentado para dar una explicación del diseño de la maquina experimental.

El objetivo de los resultados experimentales que la maquina proporcionará es un mejor conocimiento de los procesos que causan la expansión álcali-sílice. Esto ayudará con el perfeccionamiento de los actuales modelos de predicción de expansión y también en la creación de nuevos modelos. Por lo tanto se proporciona un breve análisis de algunos de los principales modelos que describen esta expansión, para ver que uso tendrán los resultados experimentales provenientes de la maquina.

La mayor parte del trabajo elaborado este año ha sido la puesta en marcha de esta máquina, con todo lo que esto involucra para una maquina única de este tipo. Las partes finales de esta tesina proporcionan información detallada sobre el funcionamiento de la maquina y el funcionamiento de cada uno de los sistemas de que la maquina depende para su funcionamiento, con información sobre su estado actual y consejos sobre su futuro operación.

Palabras claves: reacción álcali-árido, reacción álcali-sílice, modelización, estudios experimentales

Contents

1. Introduction

1.1 Overview

This thesis focuses on the assembly of the AAR tri-axial machine at the Technical University of Catalunya (UPC). In order to sufficiently explain the need for this machine, it will look in detail at the alkali-aggregate reaction and its effect on concrete structures. It will subsequently analyse the efforts thus far in understanding and modelling this reaction, and the experimental methods and tests which have been carried out in pursuit of this goal.

1.1.1 Alkali-aggregate reactions

Alkali-aggregate reactions (AAR) are chemical reactions that can occur between elements contained within concrete structures. They occur between the alkaline compounds contained within the cement and alkali-reactive substances usually contained within the aggregate. The varying nature of the aggregates used in concrete signifies that many different alkali-aggregate reactions can be observed. The most common of these is the alkali-silica reaction (ASR). (Martinez, 2010). This usually occurs between the highly alkaline Portland cement and the various siliceous substances contained in the aggregate. (Mishra, 2010). This reaction produces a hygroscopic gel, which absorbs water and swells, causing cracking to occur as tension builds in the concrete structure. This gel has been studied at length, however its composition and behaviour varies as a result of the conditions and elements present in the concrete. This makes this phenomenon difficult to predict, which is why many experimental tests have been devoted to try to better understand its formation. Cracking of the concrete causes deterioration of the mechanical properties of the concrete, while also allowing the penetration of moisture and other aggressive agents which can lead to further deterioration in its mechanical properties through different processes. (Swamy, 2009).

1.1.2 AAR tri-axial machine

At the university of Colorado-Boulder in the United States, an AAR testing tri-axial machine was designed and built in 2007 to provide experimental results in order to model this reaction. The machine is designed to test the ASR under anisotropic conditions at the macro scale. It tests a cubic 150x150x150mm concrete specimen. This specimen, in the original setup, was contained in a humidity chamber which provided the necessary moisture for growth of the formed alkali-silica gel. The setup was capable of subjecting the sample to an isotropic tri-axial load up to 10MPa (220kN over an area of 225cm^2 per hydraulic actuator) and it could be kept at a constant set temperature between 30-70°C. Since its initial construction, the setup of the machine has been subsequently altered allowing it to perform a more diverse range of experimental tests. The new setup allows for an anisotropic load to be applied, with the potential for a loading of 0-10MPa in any of the three axes. The

humidity chamber has been removed; therefore the air moisture content cannot be controlled. The design does however include a system by which an alkali-rich fluid may be pumped around the surface of the sample between it and the loading plates. This solution will also keep the specimen hydrated and prevent most of the specimen from being in contact with the surrounding atmosphere, therefore reducing substantially the effect a humidity chamber would have had.

This machine was shipped to UPC in 2010 and during the 2010-11 academic year it was constructed by Joaquín Liaudat (a postgraduate student at UPC) and myself in preparation for use.

1.2 Objectives

The objective of this thesis is to give a background to the AAR tri-axial machine by explaining the ASR problem, its chemistry, the efforts thus far to model it and the other experimental techniques used to test for it. By this, it aims to show the need for the AAR tri-axial machine acquired by UPC and the slot it fills in this area of research. It goes on to give detailed information on the setting up and workings of the machine and its future use.

1.3 Contents

The first chapter in this thesis gives an introduction as to why this thesis is being written and what topics the thesis will cover.

The second chapter describes the relevant characteristics which govern the alkali-silica reaction, including the chemistry and reactions occurring during formation and expansion of the gel. It also looks at the main factors affecting this expansion which the AAR tri-axial machine is able to control.

The third chapter looks at the various methods for testing aggregates for reactivity and potential for expansion problems in the lifetime of the concrete due to the alkali-silica reaction. These tests are important as they identify the potential reactivity of an aggregate, and are a prelude to further tests of the type conducted using the AAR tri-axial machine.

The fourth chapter looks at the proposed models for prediction of the ASR, which leads on to the need for experimental results of the type offered by the AAR tri-axial machine acquired by the Universitat Politécnica de Catalunya.

The fifth chapter describes the workings and assembly of this machine and describes its current state, while giving guidance on future operation.

The final sixth chapter summarises the work carried out this year, and offers some conclusions on the future role the experimental machine will be able to perform.

2. Relevant characteristics of the alkali-silica reaction

2.1 An overview of the alkali-silica reaction

The alkali-silica reaction attacks concrete via the degradation of the silica in the aggregate by OH^- ions followed by the absorption of positively charged ions to balance the negative charge left by this process. This creates a gel, known as the alkali-silica gel. The gel as a whole takes up more space than its constituents. The main source of expansion occurs when it is in contact with water and it takes this water in causing a further increase in volume. This can exert sufficient pressure to crack the aggregate particles and the surrounding cement paste. The gel formed is very viscous, and though its exact viscosity varies on the chemicals present during its formation, it is generally capable of progressing along the cracks formed. Providing there is an adequate water supply the gel keeps taking in water, expanding, exerting stresses on the concrete structure and moving along the formed cracks until the cracks reach the outer surface of the structure. In unloaded concrete, the cracking seen on the exterior surface of the concrete is irregular, and is termed “isle of man” cracking. This cracking, even if it does not reach the surface, causes a degradation in the material properties of the concrete, making it weaker and therefore more unsafe if in a loadbearing position.

2.2 Factors affecting the alkali-silica reaction and control of these using the AAR tri-axial machine.

There are three main factors which affect the alkali-silica reaction in a given concrete. These are the available moisture in the concrete, the temperature, and the presence of confinement stresses acting on the concrete. The AAR tri-axial machine directly controls the temperature and confinement stresses, and the moisture content can be maintained by the fluid delivery system that keeps an alkaline solution next to the concrete sample being tested. The necessary alkali OH^- ions are provided by the Portland cement and so availability of these is not a limiting factor. The size of the aggregate is also a factor; however this affects the progression of the ASR over various different concrete samples with differing aggregate sizes. This thesis will not focus on this effect; however multiple tests could be conducted under identical conditions to identify the effect this has. A similar study has been conducted by Suwito et al. (2002) whose aim was to find the Pessimum size effect of ASR in concrete. A section of this included finding the aggregate particle size which caused the maximum expansion (known as Pessimum expansion).

2.2.1 Effect of moisture content.

The moisture content is very important to the development of the alkali-silica reaction because the gel requires moisture for expansion. A lack of moisture has a limiting effect on the growth of the gel, though past a certain limiting moisture content, further increase will not lead to an increase in gel growth. One of the main examples of the damage caused by

the ASR is in dam structures, where due to the reservoir on one side of the dam, after a few years the pore space becomes saturated, leading to ideal moisture conditions for the development of the ASR. The AAR tri-axial machine has no direct moisture control system, however the delivery system for the alkaline solution to the sides of the concrete sample could be used to maintain a moisture content high enough to prevent moisture becoming a limiting factor in the reaction.

2.2.2 Effect of temperature

The temperature affects the speed of development of the alkali-silica reaction. Raising the temperature accelerates the expansion, though it is important to note that the final expansion is not increased – raising the temperature just accelerates the process. The final expansion is often the same, though in some cases accelerated tests can lead to lower values of final expansion. Figure 2.1 below shows the difference in the rate of expansion between a laboratory sample at 38°C and a sample contained within a dam at an average temperature of 7°C (Saouma & Perotti, 2006).

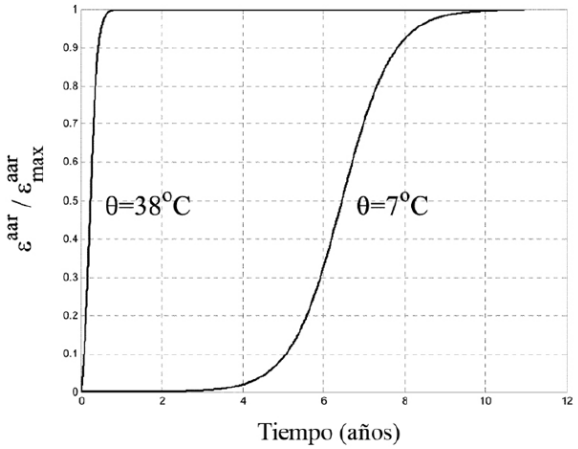

Figure 2.1 The effect of temperature on the rate of reaction

The AAR tri-axial machine has a heating system and several precise thermometers, which together are capable of maintaining the concrete sample at a set temperature between 30 and 70°C for the duration of the test, to an accuracy of 0.1°C.

2.2.3 The effect of confining stresses

In order to look at these effects, it is helpful to look briefly at the behaviour of concrete under loading without the effects of the AAR. Concrete under loading deforms due to two processes: short term, recoverable, elastic deformations; and long term non-recoverable deformations due to concrete creep. The short term deformations are straight forward to calculate using Formula 2.1:

$$E = \frac{\sigma}{\varepsilon} \qquad (2.1)$$

where E = the Young's Modulus (in MPa), which for concrete $E = 4700\sqrt{f'_c}$
σ = stress (kN/m^2)
ε = strain
f'$_c$ = specified 28-day compressive strength of concrete (MPa)

Concrete creep is due to plastic deformation that occurs over a long period due to stresses acting on the concrete. It is thought to be due to the rearrangement of cement particles at the nano-scale (Brehm, 2009). It is more difficult to analyse but several model exist which are able to predict its effects. Creep and elastic deformation both contribute to deformation of concrete under loading in the long term.

The combination of the expansive ASR process and deformation due to loading is not possible using superposition, as shown in Figure 2.2. This is thought to be because under high stresses, micro fissures open in the cement paste which absorb the volumetric expansion of the gel. This means that the alkali-silica reaction needs to be tested under loading, to determine how much loading slows the reaction down. Testing in this manner, it is possible to find a loading high enough that it prevents any expansion due to the alkali-silica reaction.

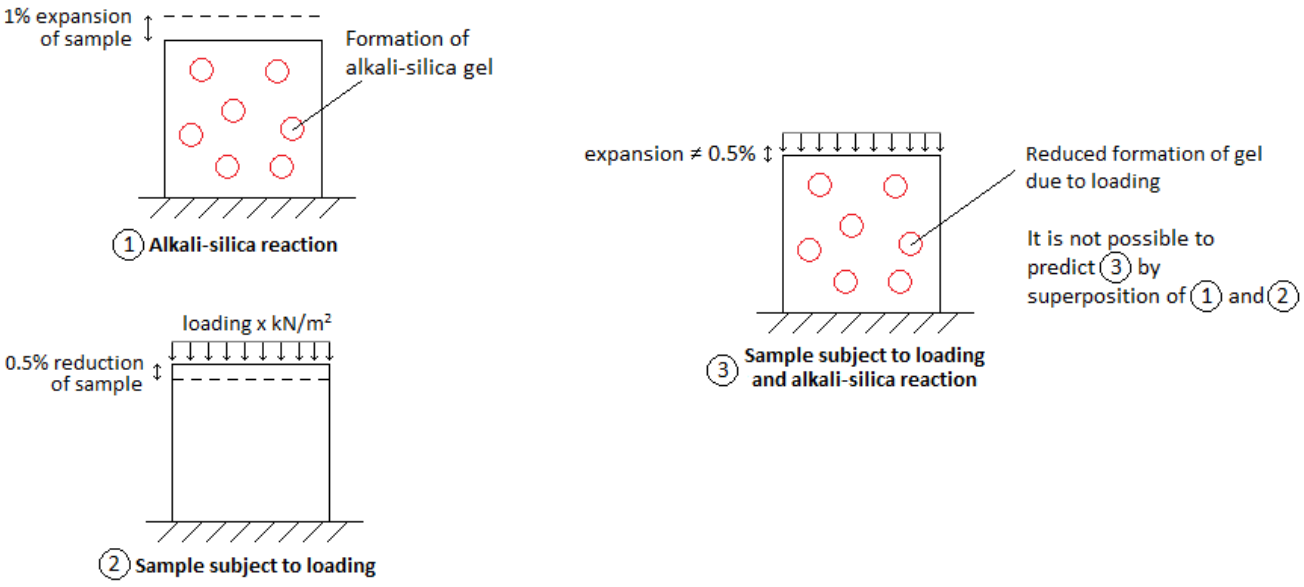

Figure 2.2 ASR under confining stresses

Figure 2.2 illustrates the ASR under confining stresses - in one dimension. This figure illustrates that the cases of the concrete under ASR expansion and concrete under load

cannot be superimposed, and therefore need to be studied simultaneously. This is part of the range of reasons why the AAR tri-axial experimental machine is necessary.

The conclusion that confinement stresses reduce the action of the ASR, can be extended to three dimensions under isotropic conditions. This corresponds to the initial setup of the AAR tri-axial machine, where the three hydraulic pistons were powered by one hydraulic pump therefore all exerted the same force on the concrete sample, subjecting it to isotropic conditions. A photo of this setup is shown in the Figure 2.3.

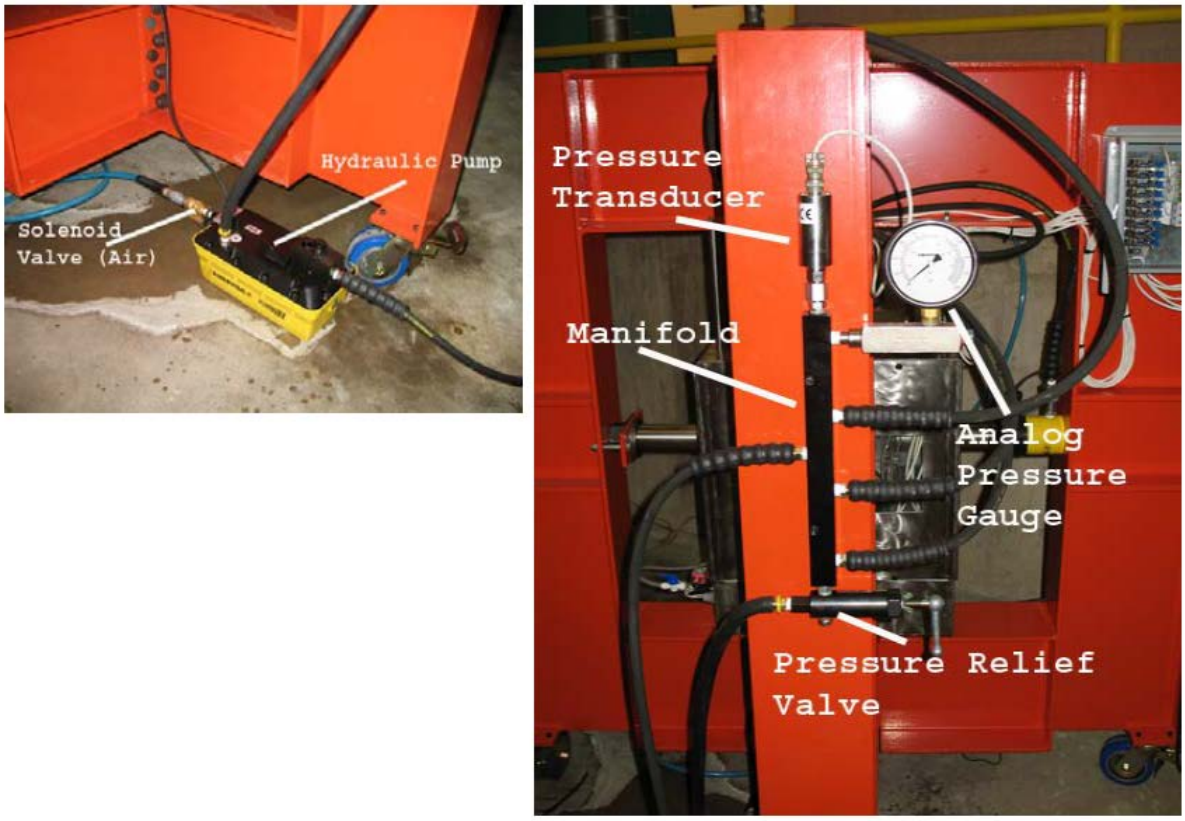

Figure 2.3 Original AAR tri-axial machine setup (Saouma & Wallen, 2007)

The specifications of the machine have since been improved allowing it to apply anisotropic loading to the concrete specimen. The new setup for the machine includes three separate hydraulic pumps, one for each axis, which enable a differential pressure to be applied to the concrete sample. This can be used to study ASR behaviour under anisotropic loading cases, an example of which is shown in Figure 2.4. In this figure, confinement stresses in the x and y plane cause a reduction in expansion in these directions (not drawn) which leads to an increase in expansion in the z direction (shown in red).

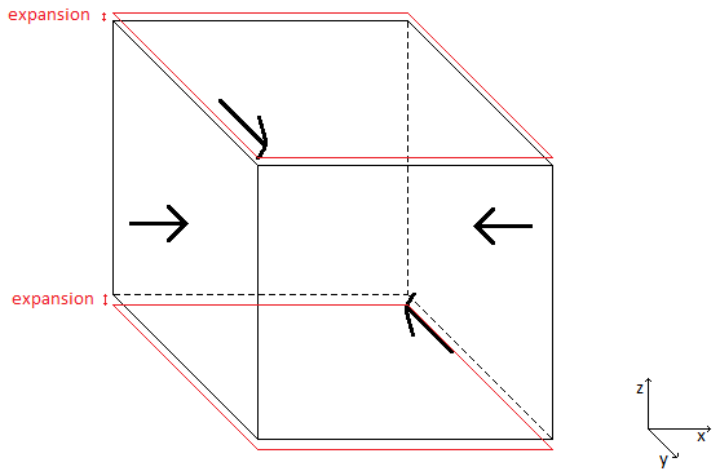

Figure 2.4 ASR under anisotropic loading

The response to this loading in Figure 2.4 depends on the loading pressure (López, Campos, & Aguado, 2011). A similar test applied only vertical confinement pressures of 5 – 10MPa, finding that vertical expansions were reduced but the volumetric expansion remained the same as for an unloaded sample. This makes sense as the gel, being viscous, expands the same amount and subsequently moves in the unconfined directions instead of the confined direction. However, for a vertical confinement pressure of around 20MPa, the volumetric expansion was considerably reduced (see Figure 2.5). The results in this figure are from a study conducted by Larive (1998). This reduction of expansion is thought to be due to the formation of micro fissures which "absorb" the formed gel. Refer to section 2.5.1 for a mode in-depth analysis of this phenomenon.

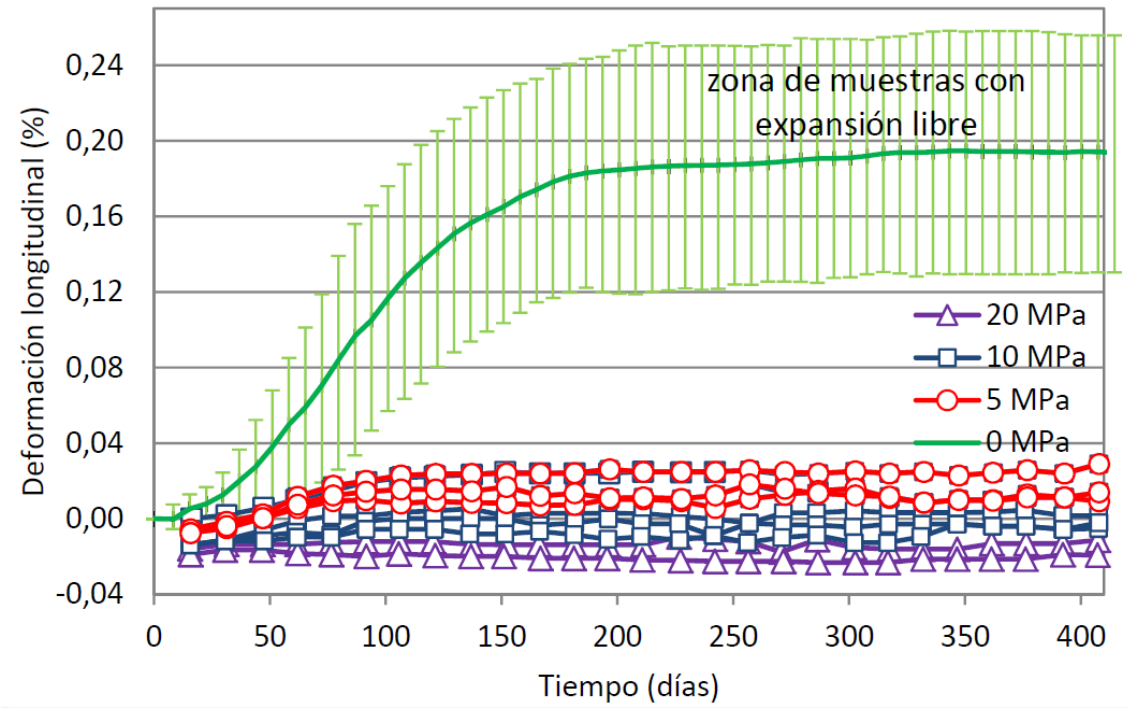

Figure 2.5 ASR under loading

An independent study, conducted by (Multon and Toutlemonde, 2005) analysed the effect of multi-axial confinement on cylindrical samples subject to AAR. Their conclusions were the same – that confinement in one direction transfers the expansion to less confined directions, with the volumetric deformation staying about the same. Their results also found a relationship between axial and radial deformation, as shown in Figure 2.6.

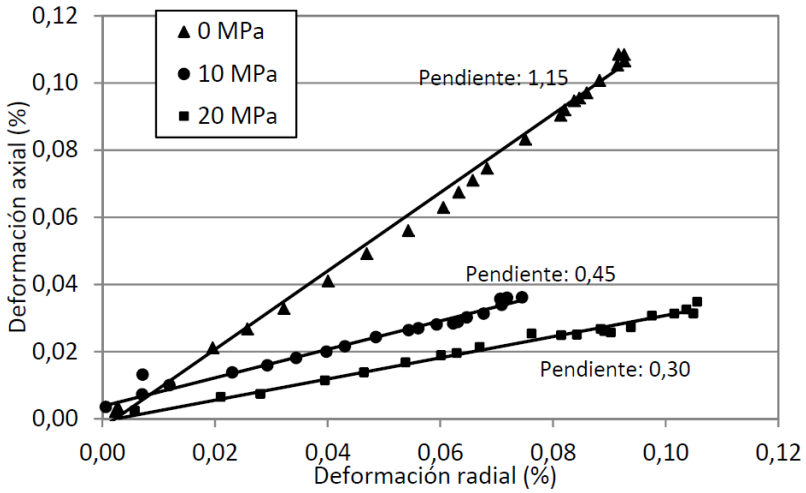

Figure 2.6 Relationship between axial and radial deformation in cylindrical samples subject AAR and radial confinement (Multon and Toutlemonde, 2005)

These finding could all easily be tested and verified - although with cubic not cylindrical samples - through future studies using the AAR tri-axial machine.

2.3 Chemistry of the alkali-silica reaction

These chemical reactions, between the alkalis in the cement (sodium and potassium) and the reactive silica in the aggregates, can be broadly broken down into two phases.

$$Reactive\ silica\ in\ the\ aggregate + Alkalis\ in\ the\ cement\ paste \rightarrow Alcali - silica\ gel$$

$$[xSiO_2] + [yNa(K)OH] \rightarrow \left[Na(K)_y Si_x O_z\right](aqueous) \qquad (2.2)$$

$$Alcali - silica\ gel + water \rightarrow expansion\ of\ the\ alkali - silica\ gel$$

$$\left[Na(K)_y Si_x O_z\right](aqueous) + [H_2O] \rightarrow [NaK_y Si_x O_z H_2 O] \qquad (2.3)$$

As the physical effects of the alkali-silica reaction are governed by chemical reactions and the consequences of these, to understand the overall process it is necessary to understand the chemical reactions underpinning them. The potential for these chemical reactions is conditioned by the chemicals and mineralogical nature of the components present in the concrete (cement, aggregate, water etc) as well as the conditions the concrete is subject to (temperature, humidity, etc). (López et al. 2011).

Mass transport is an essential part of the alkali-aggregate reaction. Aggregate particles containing a nominal proportion of SiO_2 (silicon dioxide) are thermodynamically unstable in the cement environment and therefore they react (Glasser, 1992). This is accompanied by mass transport of OH^- and alkali ions. As shown in Figure 2.7, the pore fluid is the main agent of transport as it is in close contact with both the aggregate and the cement hydration products. Cement hydration products is the term used for the products of the reaction between cement and water, in which the alkalis for the ASR are found.

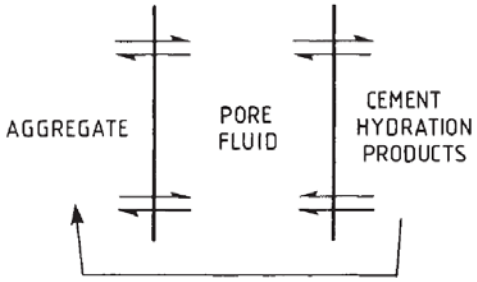

Figure 2.7 Mass transport in the alkali-aggregate reaction

This reaction is shown in more detail in Figure 2.8, which is intended to give an impression of the various reactions which occur at the surface of an aggregate particle. The cement microstructure is shown – it consists of solid hydration products, of which the figure shows two: platelets of $Ca(OH)_2$ and C-S-H (carbon, sulphur and hydrogen) structures, which are the bundles of fibres. These are not shown to a set scale, and in reality they do not occupy much space leaving a considerable amount of pore space. The surface of the aggregate particle is shown as hydroxylated. Hydroxylation is a chemical process that introduces or joins a hydroxyl group (OH^-) onto an organic compound. (Wikipedia, 2011). In this instance, the disturbed region is usually a few to tens of atoms deep. When aggregates are in a hydroxyl-rich environment, more hydroxylation is likely to occur. This process is also markedly increased by higher temperatures.

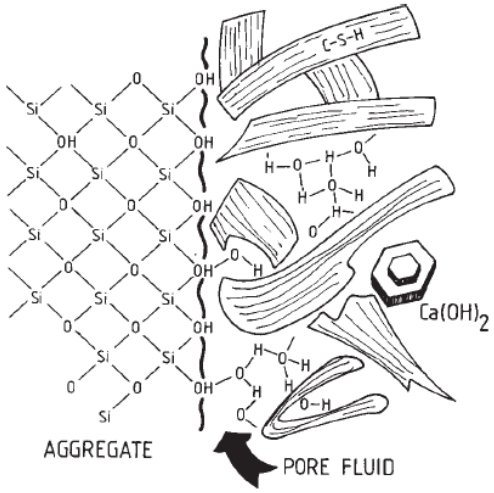

Figure 2.8 Detail of surface of aggregate during alkali-silica reaction

The alkali-silica gel formed due the alkali-silica reaction forms at this boundary between the aggregate and the region containing the cement hydration products (Dent-Glasser & Kataoka, 1981). This gel has a constitution which is not thoroughly understood at present, which then takes in water and some other elements to balance its negative charge – mainly Na^+, K^+ and Ca^{2+} ions. This gel is not very soluble, and different gels can have varying viscosities, which affects how easily the gel can move within the concrete structure.

2.3.2 Detailed chemical reactions which occur during gel formation

There are three main reactions that occur. (Glasser, 1992). The first stage involves the high pH pore fluid reacting with the S-O_2-S bonds and imbibing water – the main cause of its characteristic swelling - to form silanol bonds:

$$Si - O - Si + H_2O \rightarrow Si - OH + Si - OH \qquad (2.4)$$

These silanol bonds form in addition to any hydrous silica aggregates which already contain silanol bonding. These silanol groups are acidic, and so react with the basic cement pore fluids. These can then react again with other hydroxyls producing water:

$$Si - OH + OH^- \rightarrow Si - O^- + H_2O \qquad (2.5)$$

The second reaction then occurs. The Si-O^- (silicon monoxide) molecule, being negatively charged, attracts positive charges. This brings other mobile elements into the gel to balance the charge. Common positive elements which diffuse into the gel are sodium, potassium and calcium.

In the third reaction, more siloxane (Si-O_2-Si) bridges are attacked, producing more silicon monoxide and water:

$$Si - O_2 - Si + 2OH^- \rightarrow Si - O^- + O - Si + H_2O \qquad (2.6)$$

The gel itself has a higher volume than the reactants which comprise it, so its formation is responsible for the characteristic swelling which is so problematic when it comes to alkali-silica reactions. The amount of swelling due to gel formation is difficult to predict, because this varies depending on the composition of the gel. The density of the silica gel, as well as its water content, can be very variable which influences greatly the swelling the gel then exhibits. The elements it takes in during the second stage to balance the charge (the sodium, potassium etc) also affect its density and therefore the swelling. This is what makes predicting the gels expansion so complex.

This indefinite constitution of the gel is problematic as it changes the physical properties of the gel, making it more difficult to analyse and predict on a general level. The gels formed can vary in density from soft, readily extrudable substances to gels so viscous that they become hard, rigid materials. In real samples of concrete which has been subject to gel

formation, it has been the hard, rigid gel type which has caused the cracking to occur in the concrete; while the softer gels are the ones which can more easily travel through cracks and emerge at the surface of the concrete.

2.4 Effects of expansion on the mechanical properties of concrete

The expansive processes occurring in the ASR are usually rooted in the growth of micro fissures in the concrete. Tests carried out on the mechanical properties of a concrete undergoing the ASR show a decrease in both its Young's modulus (E) and its resistance to compression as the ASR develops. (Jones & Clark, 1998)

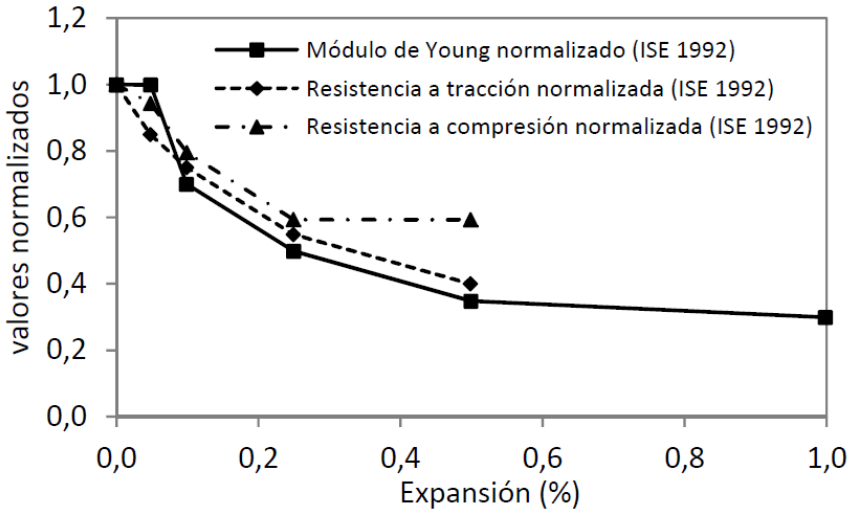

Figure 2.9 Changes in Young's modulus, tensile strength and compressive strength with ASR expansion

The changes in Young's modulus, tensile strength and compressive strength are shown as a function of the level of expansion reached by the ASR. These are shown in Figure 2.9. (López et al. 2011). It can be noted that all values show a significant reduction as expansion increases. This in particular is serious for structural concrete, which needs to maintain the strength that the structural design relied on.

2.5 Fissures in concrete due to ASR expansion

2.5.1 Microfissures

As the ASR process is expansive, pressure is exerted on the surrounding concrete paste and tends to cause microfissures which radially propagate around the affected area. Figure 2.10 shows fissuring at the aggregate boundary and in the cement paste, caused by the AAR expansion. (López et al. 2011). Fissuring at the boundary between the aggregate particle and cement paste is shown in blue, while fissuring in the cement paste is shown in yellow. Lenses where the alkali-silica gel has formed are highlighted in red.

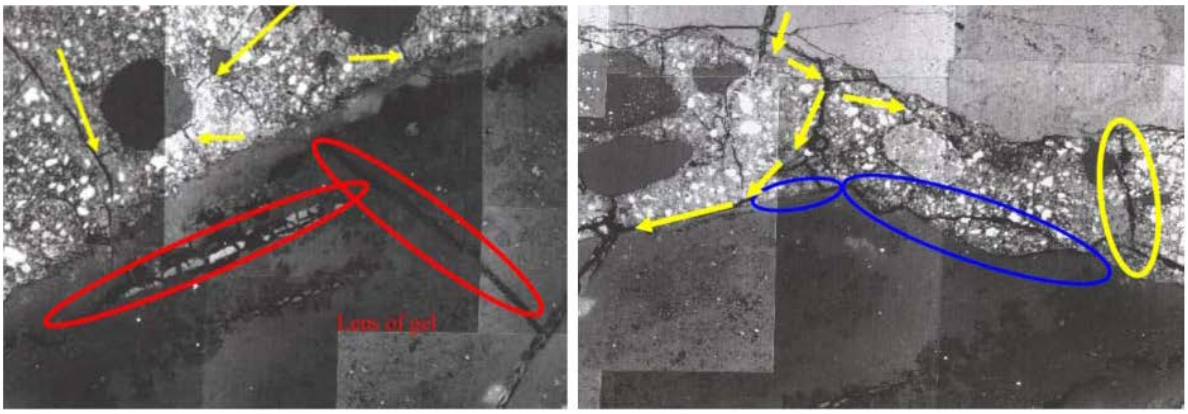

Figure 2.10 Fissuring at the concrete-aggregate boundary

2.5.2 Macrofissures

These are the fissures on a larger level which can often be visible at the surface of concrete structures affected by the ASR. The cracking has a characteristic “map cracking” or “Isle of Man” cracking pattern. (Winter, 2001)

Examples of this cracking pattern are shown in Figure 2.11. The image on the left is an auxiliary structure at the Belesar dam in Spain, and the image on the right shows the characteristic crack pattern affecting a concrete step barrier on a motorway in the US.

Figure 2.11 Macrofissures at the surface of concrete suffering ASR

This characteristic crack pattern tends to occur in unloaded structures. The ASR behaves differently under load, as detailed in a later chapter of this thesis. Cracking can still occur, however the shape of the cracks will be influenced by the loading.

3. Testing aggregates for their potential to suffer from ASR expansion.

3.1 Overview of testing aggregates for the alkali-silica reaction

There are two main classes of test for determining the susceptibility of aggregates to the alkali-silica reaction. These tests are designed to establish the potential reactivity of aggregates and cement-aggregate combinations. In these reactions, the cement constitution is treated as constant; therefore reactivity with it can be tested with a range of aggregates. These tests are performed on samples without loading, and measure the expansion of the sample with respect to time. All laboratory testing in this field is difficult, as test results can be inconclusive and it can be difficult to pin down the precise reaction causing expansion; nevertheless laboratory testing is an essential tool in understanding this phenomenon. Temperature, the nature of the solution in which the sample is contained, and the alkali content of the concrete all have a major influence on the results of the test. There are several standard tests which have been established over many years, as well as newer tests which aim to achieve results more quickly. Most of these newer methods rely on temperature and pressure to speed up the reaction. This tends to lead to higher values of expansion than those obtained with traditional methods. (Swamy, 2009).

3.2 Conventional mortar/concrete tests

There are three traditional tests which have been used to evaluate the potential reactivity of aggregates. These are the mortar bar test *(ASTM C227)*, the Canadian concrete prism test *(CSA A23.2-14A)* and the chemical method *(ASTM C289)*. All these tests have been shown to have problems but nonetheless if interpreted carefully by an engineer with knowledge of the subject they can yield comparable results.

3.2.1 Mortar bar expansion test

Mortar bar expansion tests involve storing of mortar bars in containers. The aim of the test is to test the susceptibility of cement-aggregate combinations to expansive reactions. (Farny & Kerkhoff, 2007). The expansion is measured over one year. It has been shown that the presence of wicks substantially reduces the expansion seen in the sample as shown in Figure 3.1. This reduction in expansion is due to leaching of alkalis out through the wicks. Therefore, to conduct a successful mortar bar test it is essential to remove the wicks from the containers, or seal the specimens in plastic bags. At the end of the test, the amount of alkalis remaining in the cement should be approximately proportional to the expansion observed. It is interesting to note that larger specimens experience higher expansions.

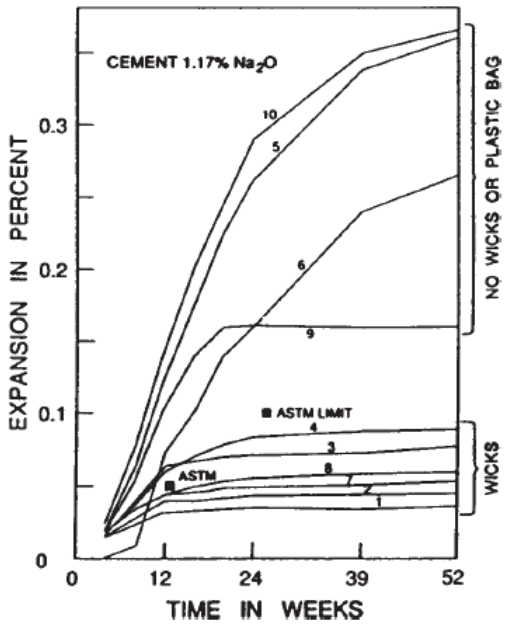

Figure 3.1 Influence of the presence or absence of wicks on mortar bar expansion tests (Swamy, 2009)

3.2.2 Concrete Prism test

The concrete prism test (CPT) is also designed to determine the potential ASR expansion of cement-aggregate combinations. It is strongly influenced by the water-cement ratio, cement content, temperature and humidity of the storage container, as well as the fineness of the aggregate particles. This means that in order to obtain comparable results, these factors all need to be carefully controlled. The cement content in particular, if very high, can lead to non-reactive aggregates being classed as deleteriously expansive. An example of this was the classification of a non-reactive Irish limestone as reactive. Removal of the wicks in the concrete prism test, unlike the mortar bar test, leads to a significant reduction in expansion. It has been shown in tests that changing the storage conditions, which affect the leaching of the alkalis from the concrete, can change the result by 23%. (Rogers, 1990). This illustrates the fickle nature of these tests, and the real need to ensure uniformity of test conditions.

The concrete prism test can also be used for the testing of aggregates which cause slow expansion. These reactions involve the expansion of coarse aggregate particles as well as the gel seen in the standard reaction. This reaction takes up to 10 years to be observed in concrete structures, and is difficult to observe in accelerated tests. It is normal to use concrete with 5.1 kg/m3 Na2O eq. in normal speed ASR expansion tests, however in tests where expansion is slow, using around 9 kg/m3 Na2O eq. at 38°C leads to expansions of the slow type being observed.

3.2.3 Chemical test methods

Chemical test methods are used when there isn't the available time to perform mortar bar or concrete prism tests. They can yield successful results, however the major limitation is

that there is no universally applicable chemical test, as each different chemical test is suited to a particular type of aggregate and so comparing tests requires both aggregates being compared to be testable using the same chemical test.

3.3 Rapid test methods

With the aforementioned traditional methods, results take approximately one year to obtain, which in a fast-moving industry can be too slow. Traditional methods are also not suited particularly to slow-reacting aggregates. There is a need to develop and standardise rapid test methods, in order to be able to achieve quicker results, comparable results and results for slow reacting aggregates. Rapid test methods aim to speed up the slow rate of the alkali-silica reaction using a combination of heat and/or pressure. There have been many rapid test methods proposed, however none of these has yet become standard. Several studies carried out have identified the potential of the NBRI 14-day method. (Swamy, 2009). This method, developed by Oberholster and Davies (1986), is based on the mortar bar method; however the bars are exposed to a 1 M NaOH solution at 80°C for 14 days. The expansion is measured with the bars still at this temperature. Expansion limits suggested are: 0.10% for innocuous aggregates, 0.10–0.25% for slowly expansive aggregates. Tests show these expansion limits to be accurate, and in a test carried out comparing the available rapid test methods, this was the only one that could accurately identify all of the reactive aggregates. (Hooton & Rogers, 1988)

4. Modelling expansions due to the alkali-silica reaction

The expansions caused by the ASR generate a new set of stresses within the concrete which, depending on their magnitude, can lead to changes in its structural behaviour. Models attempting to simulate this complex process are based in a series of hypothesis and simplifications. There are several models which attempt to reproduce this effect, from simple ones where deformations are applied linearly as with temperature deformations, to more complex models which take into account the diverse factors which influence the expansion and the changing properties of the concrete as the expansion occurs.

A report by (Saouma & Xi, 2004) classifies models into three types. The smallest, micro scale models simulate the phenomenon at the micro scale (1µm, or 10^{-6}m). This is approximately the scale of the Portland cement mortar. Meso scale models consider the two primary constituents of concrete – the concrete paste and the aggregate particles contained within it. The largest, macro scale models, simulate the global effect on the whole of the structure.

The ASR tri-axial machine is designed to test samples 150mm across, which fall clearly into the macro scale models category. However the other two categories, micro and meso scale, are interesting models to note as they function based upon several of the same principles albeit at a different scale. In addition, an understanding of the functioning of models at a smaller scale leads to a greater understanding of the processes occurring when modelling at the larger scale. It is for these reasons I have included below details on all three model types.

4.1 Micro scale models

4.1.1 Delft Lattice Model (Schlangen & Çopuroğlu, 2007)

A micro scale model proposed by (Schlangen & Çopuroğlu, 2007) is based on a lattice type model (the Delft Lattice Model), in which the aggregate structure is modelled using images of a real sample suffering the ASR prepared using the mortar bar accelerated test method. The model was created using 4200 small beam elements able to transfer normal forces, shear forces and bending moments. The simulation of the fracture is then carried out by performing a linear elastic analysis of the lattice under the expansive forces exerted by the growth of the alkali-silica gel. A certain threshold for elements was imposed, modelling the failure threshold; any small beam element subject to forces above this was removed from the model.

The model they created had a single aggregate particle, surrounded by cement paste. To run the model, a swelling alkali-silica gel was placed in three places – inside the aggregate particle, at the boundary between the aggregate and the cement paste, and within the cement paste. To simplify the analysis, these three gel locations are assumed to expand at the same rate.

Table 1: Strength and stiffness of components used in lattice simulation

	Aggregate	Dissolved edge of Aggregate particle	Interfacial transition zone	Cement matrix	ASR gel
Strength	7.0 - 13.0 MPa	1.0 - 2.0 MPa	1.5 - 2.5MPa	3.0 – 5.0 MPa	1.0 MPa

Strength and stiffness values for the lattice elements were taken from Table 1, and random values within the ranges stated were used for each element.

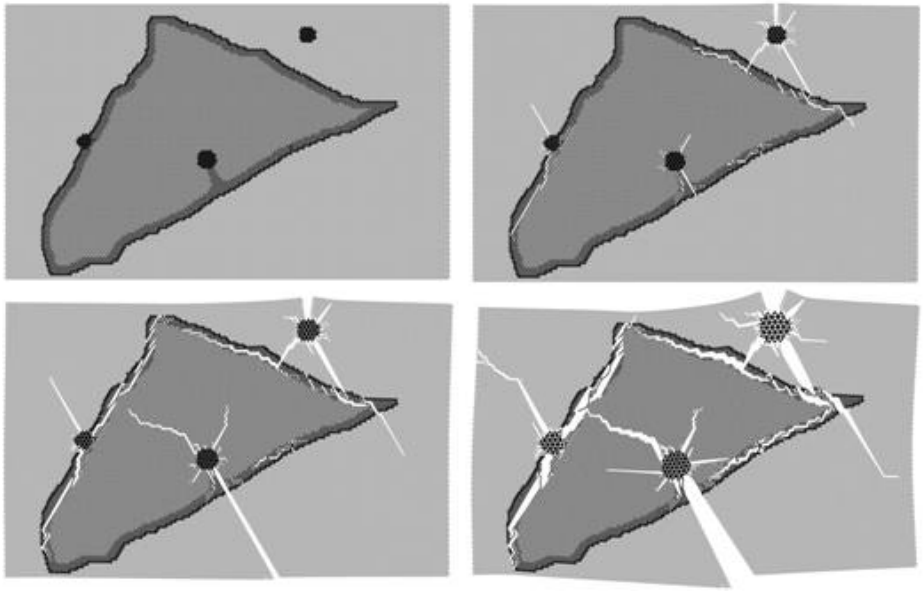

Figure 4.1 Simulation results from model based on Delft Lattice model (Schlangen & Çopuroğlu, 2007).

The results from this simulation are shown in Figure 4.1. They correspond well with the real ASR cracking expansions noted in the real sample subject to the accelerated mortar bar test method. (Schlangen & Çopuroğlu, 2007).

4.1.2 Mathematical Model (Suwito et al.)

An alternative model was developed by (Suwito, W.Jin, Xi, & Meyer, 2002). The aim of their model was to find the Pessimum expansion due to the ASR in concrete. Pessimum expansion is the maximum expansion which will be reached, and it depends on the volume fraction, type and the size distribution of the reactive aggregate, the composition and alkali content of the cement, the rate of strength development and the mixture proportions of the concrete.

Their model combined several diffusion theories. The expansive process was divided into two parts: Firstly, diffusion of the hydroxyl and alkali ions into the aggregate, followed by the reaction of these with the reactive silica contained within the aggregate. Then secondly, expansion due to the ASR once the empty pore volume next to the aggregate particle, left by reactants in the concrete setting process, has been filled by the gel.

The first of these processes happens through micro-diffusion, which can be described by Fick's law which takes into account the concentration of free ions in the pore solution inside the aggregate, the permeability of the ions in the aggregate to calculate the binding capacity of the aggregate. The stages of this first process process are illustrated in Figure 4.2.

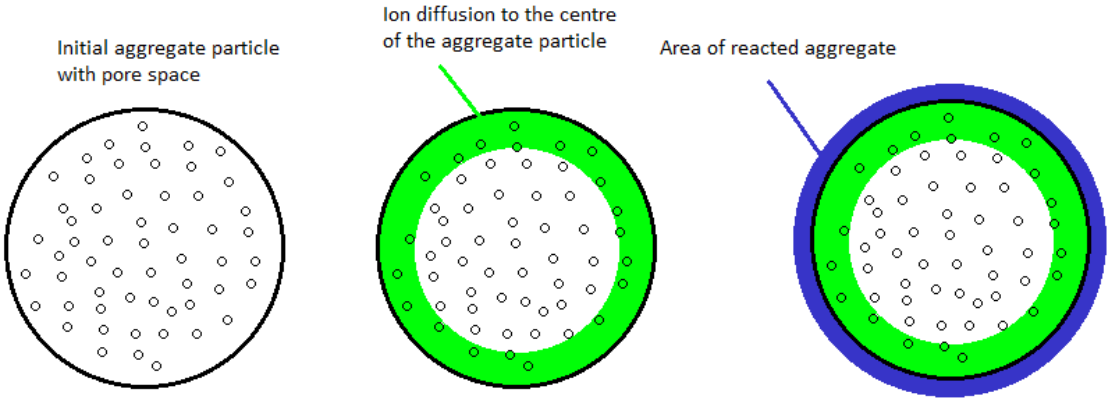

Figure 4.2 Diffusion of ions into aggregate particle

The second of these processes is due to the growth of the alkali-silica gel. There is a void space between the aggregate particles and the cement paste, which is made up of the Interfacial Transition Zone (ITZ) due to the perturbation of the concrete structure by the large aggregate particles, and the space left over from the concrete reactants. The formed gel first fills the void space, and then once it has occupied this, it starts to generate interfacial pressure which causes the gel to further permeate the pore structure of the cement paste. This leads to two variables: the volume of gel, and the effective volume of gel which is the volume which doesn't fit into the pore space and causes the stresses and expansion. Once the effective volume of gel becomes greater than zero (when the pore space has filled up), the gel starts to exert an interfacial pressure. This calculated using Darcy's law, which calculates the pressure distribution of the gel taking into account its viscosity, concentration and permeability. The change in volume is then calculated taking into account the volume change of the gel and the total volume of the aggregate. For this, the model assumes the gel exerts isotropic expansion pressures.

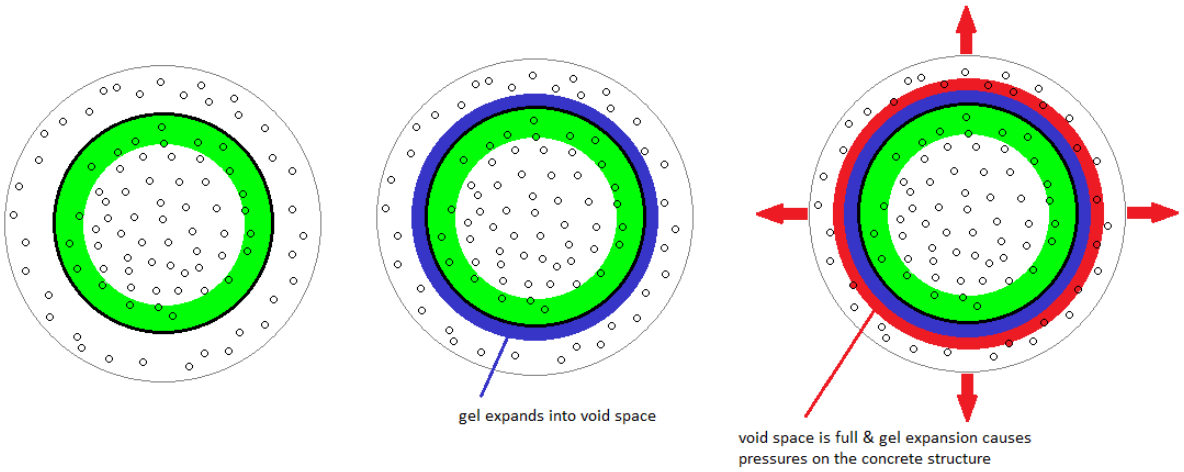

Figure 4.3 Expansion of gel applying force to concrete structure

This second stage of this process is illustrated in Figure 4.3. The second stage shows expansion of the gel within the void space therefore no pressure is applied to the surrounding concrete paste. The third stage shows the gel expansion having exceeded the limits of the void space; therefore the gel exerts an interfacial pressure on the surrounding concrete paste which causes the expansion of the concrete structure as a whole.

4.2 Meso scale models

Meso scale models represent the concrete considering its heterogeneity, modelling its two primary constituents – the aggregate and the mortar. This scale of model is often used to study the Pessimum size effect, which is the highest potential expansion for a particular aggregate particle size. This is useful to determine the worst-case particle size.

It is possible to study at the meso scale also using the lattice model discussed in 4.1.1, defining lattice elements and their properties, and removing elements once their failure stresses are reached.

An alternative report studied the deterioration of concrete affected by the AAR using a finite elements 3D computational tool. (Comby-Peyrot, Bernard, Bouchard, Bay, & Garcia-Diaz, 2009). This proposed the modelling of the two phases as discrete. Linear-elastic behaviour was assumed for the aggregates and a non-linear behaviour, taking into account damage due to gel expansion, was proposed for the mortar. The contact between aggregate and cement paste was modelled as rigid without the ability to slide, and friction and dissipation of energy at the boundary were disregarded.

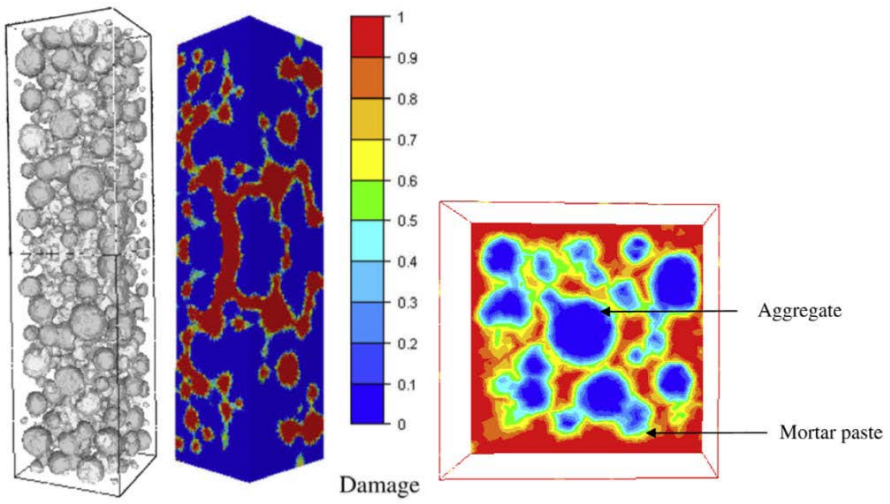

Figure 4.4 Combey-Peyrot et al, finite elements meso-scale model showing damage at the surface

This model could accurately predict the Young's modulus of the damaged concrete, and the peak resistance; however it also predicts a "softening" which is not observed in experimental tests. Figure 4.4 shows the application of this model to study the cracking and deterioration of concrete having the expansion applied in the middle of the aggregates (therefore modelling gel expansion as having occurred there).

4.3 Macro scale models

Macro scale models are to the scale of the actual concrete structures affected by the ASR, and therefore they are the most commonly used models as they predict the effect of the ASR on real structures. A summary of several important ASR prediction models is presented below. The AAR tri-axial machine is designed to yield experimental results which can be used to test the accuracy of models to the macro scale. The machine was designed and built by V. Saouma to test the accuracy of his model for ASR expansion, and a description of this model follows to give a background to the creation and focus of the AAR tri-axial machine.

4.3.1 Equivalent temperature model

This is one of the simplest ways to model expansions due to the ASR. A rise in equivalent temperature is modelled, so that the expansion of the concrete due to the equivalent temperature rise is the same as the expansion due to the ASR. This model can be adapted for anisotropic expansions, using different "thermal dilation coefficients" for the different directions. (López, Campos, & Aguado, 2011).

4.3.2 Model equating expansion speed with principal stresses (Thompson)

One of the most well-known models, created by (Thompson et al, 1994) relates the speed of expansion with the principal stresses using the following equation:

$$\frac{d\varepsilon_i}{dt} = \frac{d\varepsilon_0}{dt} - K log\left(\frac{\sigma_i}{\sigma_0}\right) \qquad (4.1)$$

where ε_i = expansion in direction i.
ε_0 = free expansion (no stresses).
K = a constant.
σ_i = the stress in direction i.
σ_0 = the stress below which the expansion is unaffected.

This model, although popular, is still relatively basic as it fails to take into account many of the factors which influence the ASR.

4.3.3 Finite element analysis of expansion

This model was proposed by (Léger, Côté, & Tinawi, 1997). This model considers some of the factors affecting the rate of expansion of the concrete. The deformation at any point is determined as a function of four factors: the confinement (F_C), the temperature (F_T), the humidity (F_H) and the reactivity of the components (F_R). These four factors are converted to variables in the range 0-1, and are input into the formula below to find the expansion at a point in the finite elements mesh.

$$\varepsilon_{aar}(t) = \beta[F_C(\sigma, t).F_T(t).F_M(t).F_R(t)] = \beta(t).CTRM \qquad (4.2)$$

Aside from the factors mentioned above, CTRM is the normalised deformation due to the factors which influence the ASR, t is time, σ is the confining stress and β is a calibration factor used to match the models predictions with experimental results.

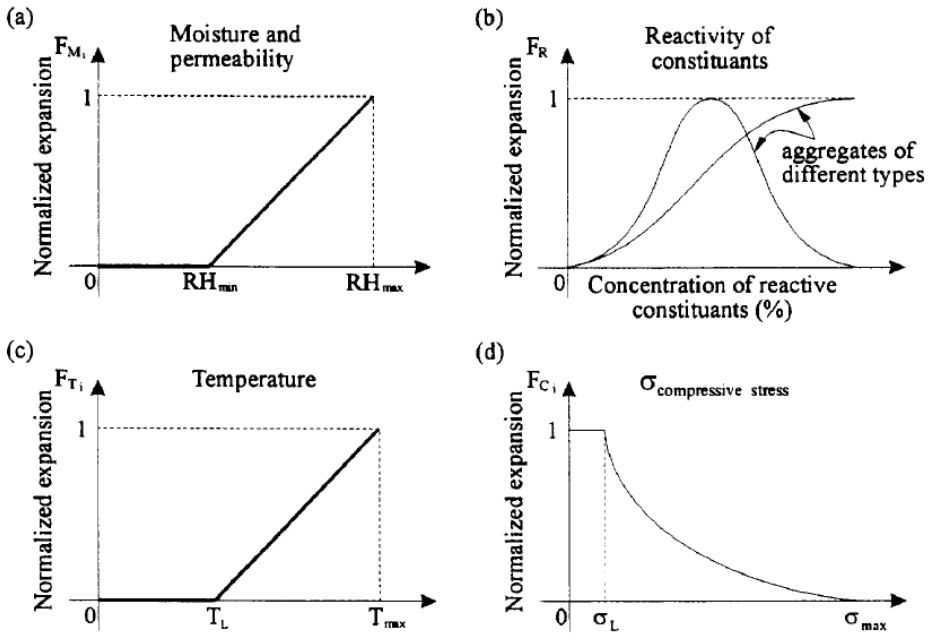

Figure 4.5 Normalised variation of the factors which affect the AAR

Figure 4.5 shows the normalised variations of the four factors used to calculate expansions at a point. The matrix of material properties is calculated considering microfissurisation and the effect of expansion due to AAR. The model calculates the material properties matrix as a function of the Poisson ratio, a creep coefficient, deformations due to AAR and total deformations as well as resistances to tensile strength and the modulus of deformation, both of which are modelled as reducing with time.

This model was used model the structural behaviour of concrete dams suffering from AAR, and proved successful although could be improved with more laboratory testing to optimise the models predictions, as well as the development of the model to explicitly simulate the physical processes involved.

4.3.4 Combination of chemical and mechanical models

It was noted by (Bournazel & Moranville, 1997) that research had been conducted on the chemical and mechanical angles of the AAR, but little research had been devoted to combining these. They set out to develop a macroscopic model which could couple the two. Similarly to the Leger model detailed previously, the AAR was considered as a function of the chemical reactions taking place, the temperature, the humidity and the confinement stress. Based on experimental results, they found a two stage relationship between the expansion (ε) and the reacted alkalis (A) shown below, where ε_0 and A_0 are both material constants. These relationships are graphically represented in Figure 4.6, which shows the relationship between the reacted alkalis and the deformation.

$$for\ A < A_0 \qquad \varepsilon_{aar} = 0 \tag{4.3}$$

$$for\ A > A_0 \qquad \varepsilon_{aar} = \frac{\varepsilon_0}{A_0}(A - A_0) \tag{4.4}$$

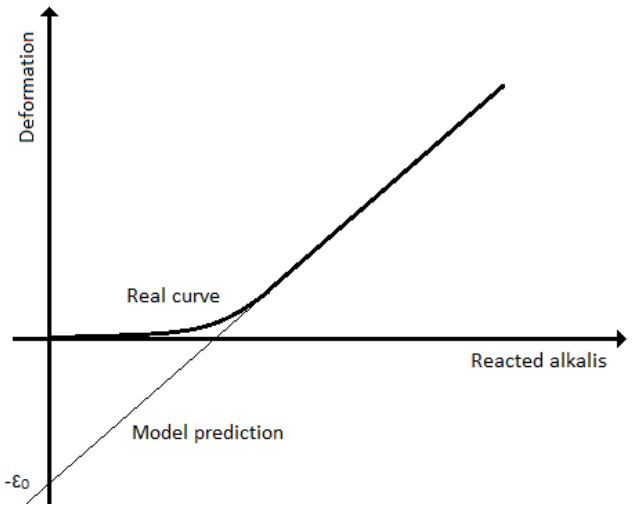

Figure 4.6 Relationship between reacted alkalis and deformation (real and model prediction).

To model the relationship between A and time, it was hypothesised that the reaction is first order and can be modelled using the law of Arrhenius. The influence of the humidity was factored in through use of a potential function by which a lack of humidity lowers the expansion, and the influence of confinement was included by way of a simplified fracture mechanics model relying on the following assumptions: anisotropic expansions, a single mode of fissure expansion (type I), no fissure interaction, and gel volume produced proportional to free expansion.

Application of this model to a sample subject with loading in only one direction of 5MPa yields the deformation results shown in Figure 4.7 for each axis:

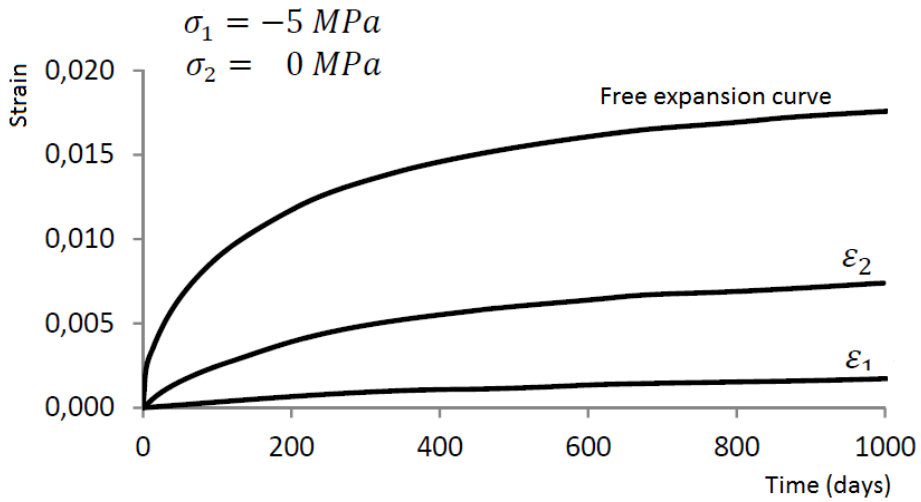

Figure 4.7 Results of Bournazel & Moranville model on a sample subject to anisotropic loading.

From figure 4.7, it can be noted that the results show a linear relationship between the expansions in the two directions (1 and 2) with reference to the free expansion curve. Other models have suggested that the total volumetric expansion should remain constant, which would suggest a reduction in the strain in one direction due to loading on one axis only should lead to an increase in strain in the orthogonal axis. This model does not seem to show this relationship. This could be due to a misinterpretation of this graph, or conflicting results between studies.

4.3.5 Other models of note

A model developed by Huang and Pietruszczak (in 1999) presented a thermo-mechanical non-linear model of concrete undergoing the ASR. This considers formation of the gel next to the aggregate particles causing progressive damage to the material. An interesting characteristic of this model is that the progress of the reaction is associated with degradation of the specimen, which is evaluated as a function of its Young's modulus and resistance to tensile and compressive forces.

Capra and Sellier (in 2002) developed a model based on a probabilistic description of the four main factors influencing ASR expansion – kinetics, temperature, humidity and

confinement. According to their model, in an unloaded concrete there exists a balance between the average pressure exerted by the gel and the stresses incurred in the material, which can be obtained through probabilistic analysis.

4.4 Macro scale model for ASR expansion by V. Saouma

This was the model that V. Saouma developed prior to the design and assembly of the ASR tri-axial machine; therefore it is likely that the machine was designed to provide results to improve the model. It is more complex than the aforementioned macro scale models. It is a thermo-chemo-mechanical model rooted in the chemistry, physics and mechanics of concrete (Saouma & Perotti, 2006). The main advancement that the model provides is the assumption of a volumetric expansion, redistribution on the basis of weights related to the stress tensor, and affectation of the reaction kinetics by the stress tensor. The model draws reference from Ulm et al (2000) and Larive (1998).

It contains two different aspects of mathematical modelling of the ASR in concrete which may be distinguished. Firstly, the kinetics of the chemical reaction and the diffusion processes involved, and secondly, the mechanics of fracture which affect volume expansion and causes loss of strength along with possible desintegration the material.

These lead to a series of equations which describe the acting processes. The fundamental equations define the reaction of the reactive silica in the aggregates with the alkalis in the cement paste to create the alkali-silica gel, and the expansion of this gel through the imbibation of water.

The model bases its approach to modelling the thermodynamic expansion with respect to time from the work of Larive (1998), who conducted a very thorough investigation into the AAR and proposed a model for the expansion with respect to time at a set temperature.

Modelling of the induced pressure due to the expansion of the gel based on the following considerations:

1) As the AAR is a volumetric expansion, and as such it cannot on be addressed individually along one axis direction – attention must always be placed on the effect this has on the other orthogonal axes.
2) Temporal variation of temperature affects the AAR and is taken into account.
3) AAR expansion is constrained by compression, and in an anisotropically loaded specimen, this reduction in expansion is transferred to the unloaded axes.
4) High compressive or tensile stresses inhibit AAR expansion due to the formation of microcracks or macrocracks which absorb the expanding gel.
5) High compressive hydrostatic stresses slow down the reaction; tri-axial states of stress slow down but do not eliminate expansion.

6) Accompanying the AAR expansion is a reduction in the material properties of the concrete, notably the tensile strength and Young's modulus.

These assumptions lead to a general (uncoupled) equation for the incremental free volumetric AAR strain, which is the basis of this model. The model was calibrated and values of constants were determined by comparison with experimenal results obtained by Multon et al. (2003), who performed extensive large-scale testing of the ASR in reinforced beam specimens.

Simulation using this model leads to an overestimation of stresses, as the model assumes plain strain conditions in two directions without allowing the redistribution of stresses over the third direction. For further refinement of the model, simulation would need to be possible in three dimensions, requiring far more computing power as current 2D model produces output files of approximately 45mb. The model however represents one of the most comprehensive attempts to date to quantify and describe through equations the important chemical, thermal and mechanical process affecting expansions.

The usage of this model to date has been for dam analysis. It can be tentatively hypothesised that a role for the AAR tri-axial machine relating to this model could be in testing of the model at a smaller (though still macro) scale. This would allow closer examination of the ASR reaction using the models main inputs (temperature, humidity, and anisotropic or isotropic pressure) in order to better model the specific reaction stages at this smaller scale. Information from these tests could then be used for refinement of the model.

5. Design and Assembly of the AAR tri-axial machine.

Figure 5.1 Overall components of the AAR tri-axial machine

5.1 Background to the machine

The AAR tri-axial machine (Figure 5.1) is designed to fill a gap in the testing so far carried out in the engineering community on the ASR under tri-axial anisotropic loading. It is designed to be able to subject a cubic specimen of size 150mm to an anisotropic load of up to 10MPa, definable for each of the three axes. This enables loading to be applied independently to each axis, and therefore the behaviour of the reaction under diverse loading conditions can be studied. It is also capable of maintaining the temperature of the specimen constant, between 30-70°C, to a precision of 0.1°C. In addition, it supplies an alkaline solution at the contacts between all of the loading plates and the specimen itself, which provides the OH^- and water stimulating gel growth, and attempts to keep the conditions at the edge of the sample homogeneous with the interior of the sample.

5.2 General assembly

Upon arrival, one of the arms on an active loading plate had broken – this was welded back into place but care will need to be taken when installing the LVDT extensions to ensure that it has been welded correctly and that it isn't influencing results at all. It shouldn't, as the LVDT strain readings are zeroed before any test, however it is worth bearing in mind. The damage is shown in Figure 5.2.

Figure 5.2 Damage to loading plate arm

Before assembly began, changes to the setup had to be made in accordance with the environment the machine was to be working in. In Colorado, the machine was situated on a concrete surface of which little care had to be taken; however here in Barcelona the machine was to be in a soil mechanics laboratory which had initially been designed as office space, therefore the floor was not directly suited for the machine. In lieu of this, a metal support plate was constructed in a nearby laboratory and painted with a grey anti-rusting paint. This was important to distribute the load from the wheels, as the laboratory was designed just as office space and therefore not for heavy items; and furthermore to catch

any drips and spills of oil, alkali solutions, etc which were more than likely to occur during the operation of the machine. The setup is shown in figure 5.3, with an inlaid image of the original setup.

Figure 5.3 Metal support tray, with inlaid image of original setup in Colorado.

As the machine originally ran on the US voltage of 120V, all electrical components had to be checked for compatibility. Most of the components could work on either the US or European voltages, but some of the heater controls were unable to run at this voltage so a transformer was installed into the enclosure with the heater control system. This needed to have a power of >900 watts to power the six 150watt heaters.

5.3 The load frame

The load frame comes in three separate pieces. It is used to provide the reaction forces that allow the hydraulic pistons to apply force to the concrete specimen. It is constructed of United States standard W12x24 I-beams, designed to deflect less than 0.25mm under the full 220kN confinement load. This is verified in Figure 5.3:

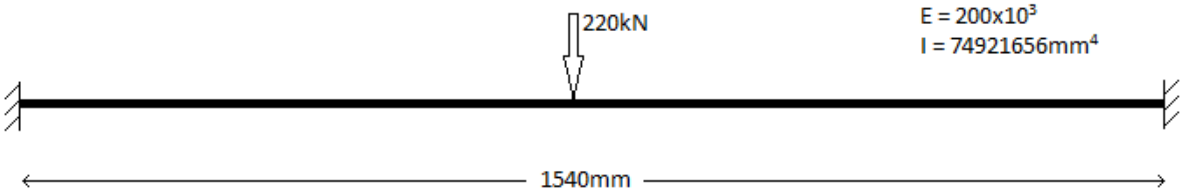

Figure 5.1 Verifying beam deformation

$$\delta = \frac{Pl^3}{192EI} = \frac{220 \times 10^3 \times 1540^3}{192 \times 200 \times 10^3 \times 74921656} = 0{,}25mm \qquad (5.1)$$

The load frame is electrostatically coated with a red plastic powder coating, which protects the frame from corrosion. Upon arrival at UPC, the frame had several large patches where the coating had peeled from the frame, leaving the metal exposed. This was re-painted to avoid damage to the frame.

Construction of the frame is straightforward, although the components are heavy. The three components are bolted together at the top and the bottom of the assembly. The bottom two bolts at the top are best left undone until assembly of the machine is complete, so as to be able to attach the top hydraulic actuator. These bolts use Allen keys with Imperial sizes.

5.4 Hydraulic loading system

The hydraulic loading system is controlled fundamentally through the LabVIEW computer software. Air at a constant pressure, from the laboratory supply, is admitted in short computer-controlled bursts via a direct-acting solenoid valve into the hydraulic pump. Controlling the duration of the bursts and the time interval between them permits a controlled rise in the pressure which drives the hydraulic actuator. The setup of the hydraulic pumps is shown in Figure 5.4

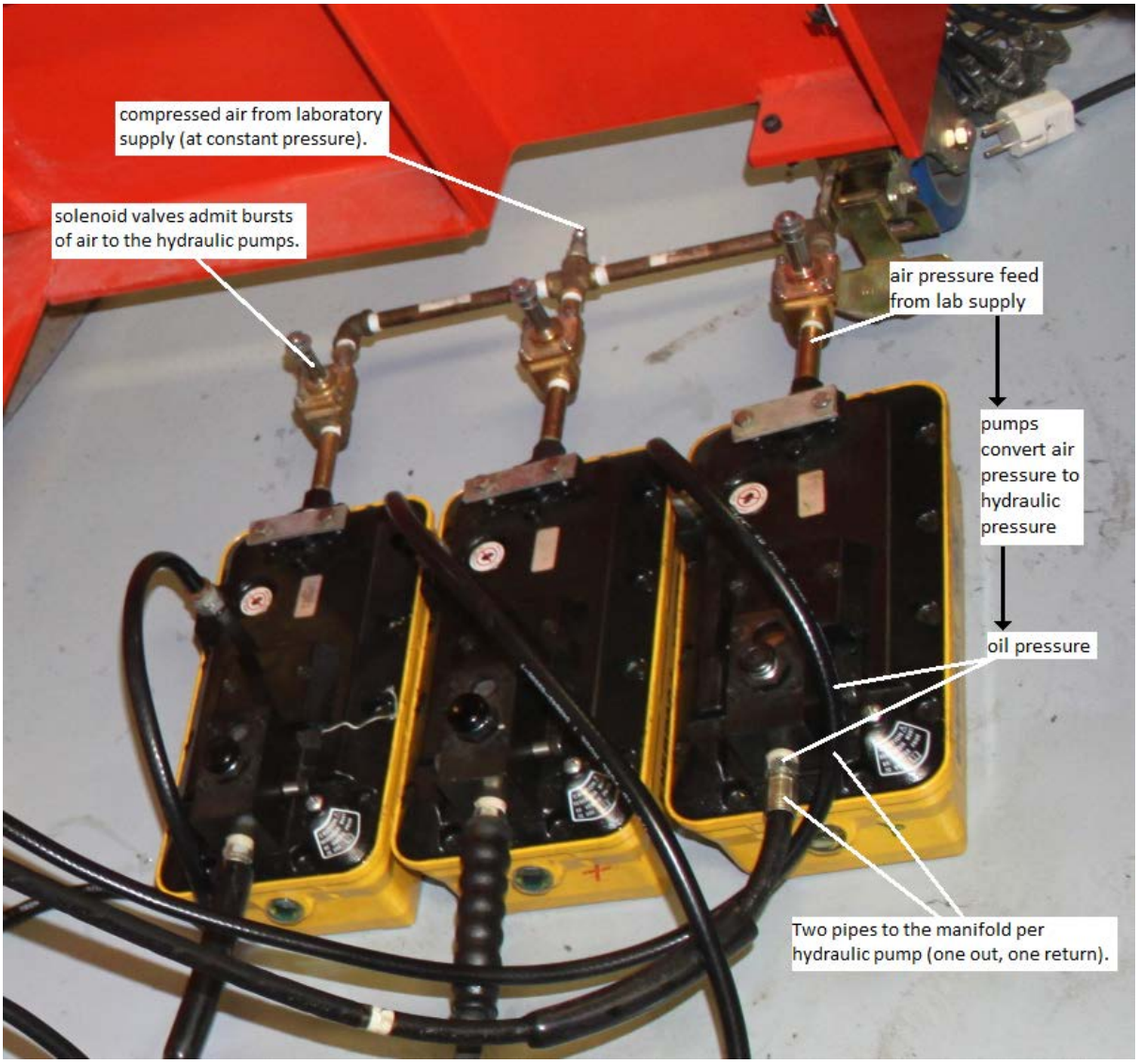

Figure 5.4 Hydraulic pumps

The hydraulic systems main feature is the manifold, shown in Figure 5.5. This is connected to three hoses; two to the corresponding hydraulic pump and one to the hydraulic actuator. It also has one manual pressure relief valve and two pressure indicators; one analog indicator which is used when adjusting the manual pressure relief valve, and one digital gauge which sends a signal to the computer controlling the pressure.

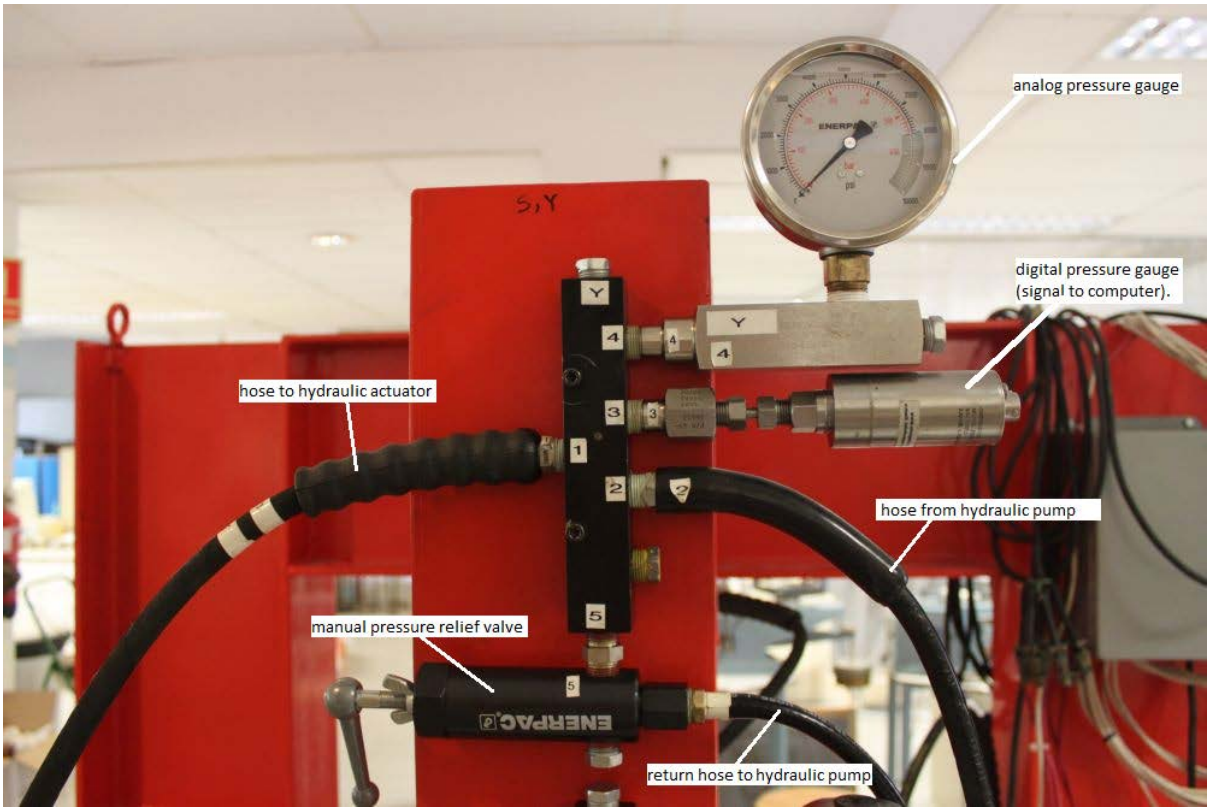

Figure 5.5 Hydraulic manifold

The whole hydraulic system is represented in the schematic (Figure 5.6):

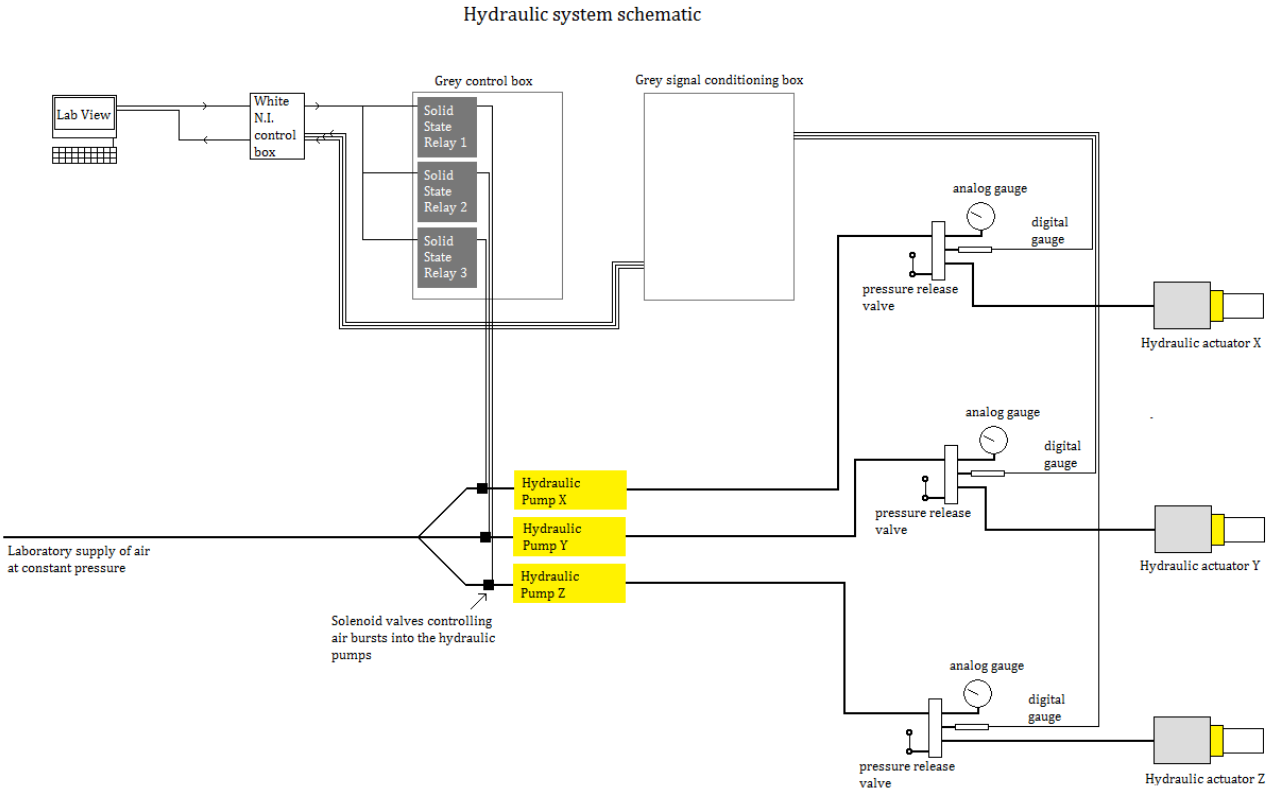

Figure 5.6 Hydraulic system schematic

In order to begin the assembly of the hydraulic system, it was necessary to acquire oil to replace that lost in transport and the processes of disassembly and assembly. This oil is H-95-Y oil bought from Sutec S.A., Barcelona.

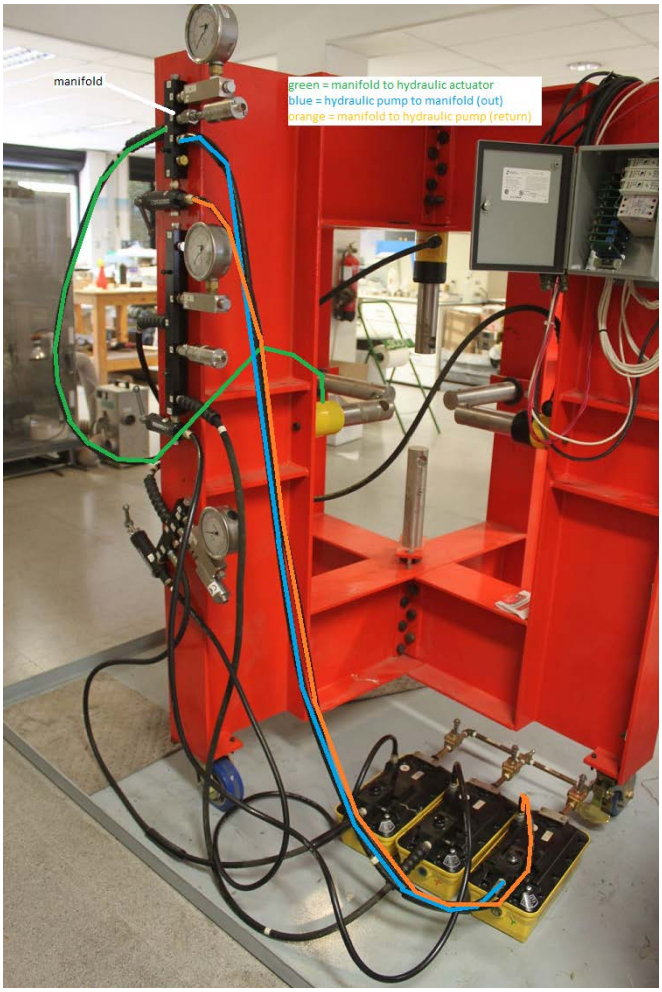

Figure 5.7 Guide to hose assembly

Filling of the hoses must be done in a certain order, as not all of the hoses can freely screw at their ends. From Figure 5.7, first the blue hydraulic pump to manifold (out) hose needs to be connected to the hydraulic pump, filled with oil, and then connected to the manifold. This hose needs to rotate fully in order to screw into any connections, and so to connect it to the manifold requires the removal of the manifold from the main frame and rotation of the entire manifold assembly. Next, the (orange) manifold to hydraulic pump (return) is connected, and finally the (green) manifold to hydraulic actuator is connected. This is the easiest to connect, as it features a valve system on either end which prevents the escape of oil when not connected.

Filling the hoses with oil requires the hose to be held upright, and oil to be slowly poured in through a funnel. It needs to be poured a few drops at a time, and shaken constantly, in order to allow any air bubbles to escape. This process can take 45 minutes or more per hose, requires two people to complete and is easiest if it can be done with both ends of the

hose free. This way filling can be alternated between either end, and raising or lowering the each end with respect to the other facilitates the escape of air bubbles as well as allowing you to see how far you have filled the hose.

5.5 Measurement of deformations using LVDTs

The deformations of the system are measured using Linearly Variable Differential Transformers (LVDT's). A schematic of an LVDT is shown in Figure 5.8. Each pair of loading plates has three LVDT's that measure the deflection between them. LVDT's sense the distance to the opposing plate using threaded extension rods which are attached to the opposing plate. On the end of the extension rods, an LVDT core is mounted so that it floats within the LVDT body.

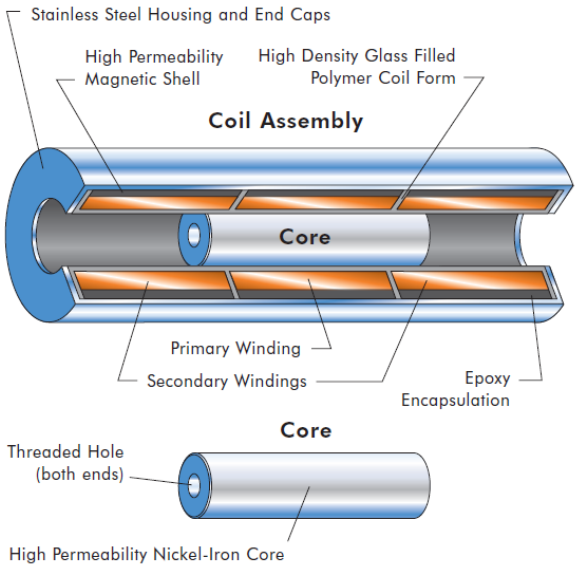

Figure 5.8 LVDT schematic (Macro Sensors, 2003).

When deformation occurs due to specimen expansion, the core moves an equal amount relative to the LVDT. The primary winding of the LVDT is energised by a constant amplitude AC source from the signal conditioning equipment. The developed magnetic flux is coupled by the core to the adjacent secondary windings. Changing the location of the core varies the voltages induced in the two secondary windings, and comparing these voltages allows for a precise determination of the core location (Macro Sensors, 2003). This voltage is interpreted and logged by the computer in LabVIEW. The layout of the LVDT's for a pair of load plates is shown in Figure 5.9.

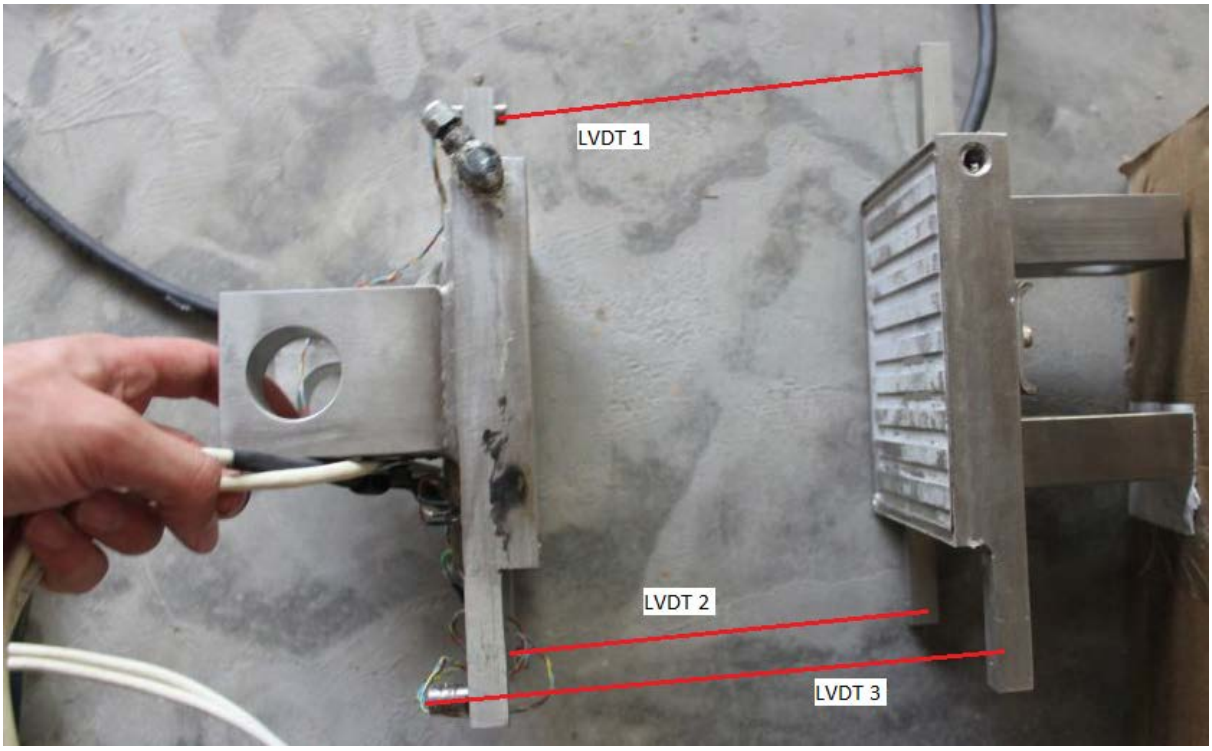

Figure 5.9 LVDT placement

The LVDT cores and extension rods were unfortunately not included in the original delivery of the machine, and the cores in particular are very expensive to obtain in Barcelona. A set of cores was obtained by Ignacio Carol on a trip to Colorado, and a set of extensions was manufactured in Barcelona. These extensions were fairly difficult to manufacture, as they are small and require US thread standards in order for the cores to screw into the end of the extension rods. The extension rods were required to the specification shown in Figure 5.10:

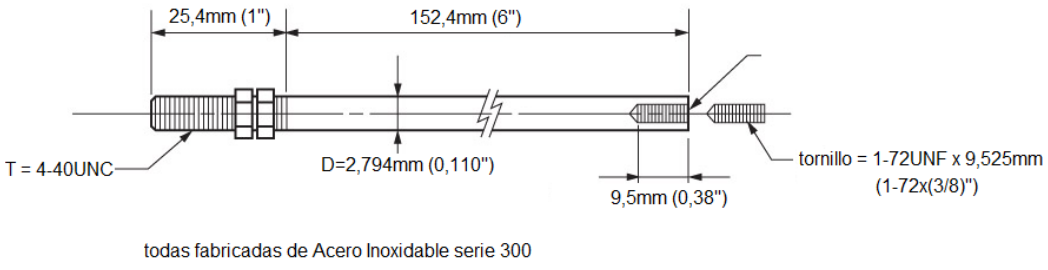

Figure 5.10 Extension rods detail

These US thread cutting parts are slow to obtain in Barcelona, and so for ease of manufacturing the 4-40UNC thread was changed to a European M3. The diameter of the extension was increased from 2.794 to 3mm. This new size still passes freely through the LVDT with no friction whatsoever and so should not be a problem. The material for the extensions was also changed from stainless steel to brass, as the initial attempts to manufacture the extensions from stainless steel failed as the small size and hardness of the stainless steel meant that the drill bits broke frequently. Using brass should not lead to a loss of precision. This is because it is not magnetic, therefore will not affect the magnetic

field through which extension is measured, and also because it is under no stress or forces therefore its softness should have no effect on the results. In any case, before use LVTDs need to be tested and calibrated and these are no exception.

After fabrication of the extensions, the staff at Colorado University found the cores and extensions corresponding to our project, and so the extensions we have fabricated here and the extra cores purchased will serve as backups should any of the original components fail.

5.5.2 Signal conditioning

To simplify the wiring, all sensors except for the LVDT's have integral signal conditioning. This means that the sensor can output voltage levels which are compatible directly with the computers data acquisition hardware. The size and performance requirements of the LVDT's necessitated the use of external signal conditioning. The LVDT signal conditioners, +/-15 Volt, +18 Volt, and +5 Volt power supplies are housed in a grey enclosure stuck to the reaction frame. All sensor wires are routed through this enclosure and then on to the white National Instruments shielded connector blocks which then connect directly to the computers National Instruments PCI 6229 data acquisition card.

5.6 Heating System

A closed-loop temperature control system is employed on the machine, in order to accelerate the alkali-silica reaction. This is capable of holding the sample at a constant temperature between 30-70°C, to a precision of 0.1°C. Each stainless steel loading plate is equipped with a 150 watt flush-mounted heating element. Figure 5.11 shows the stainless steel plate with flush heater, and Figure 5.12 shows the grey heater control box.

In LabVIEW, the user specifies the desired heat at which the specimen is to be contained. Temperature data from the sensors on the plates is compared to this desired heat, and using this, an error signal is generated which is sent to the pulse-width modulated power controller. This drives the solid state relay which enables the heaters power to be varied between 0-100%, to accurately control adjustments in heater output.

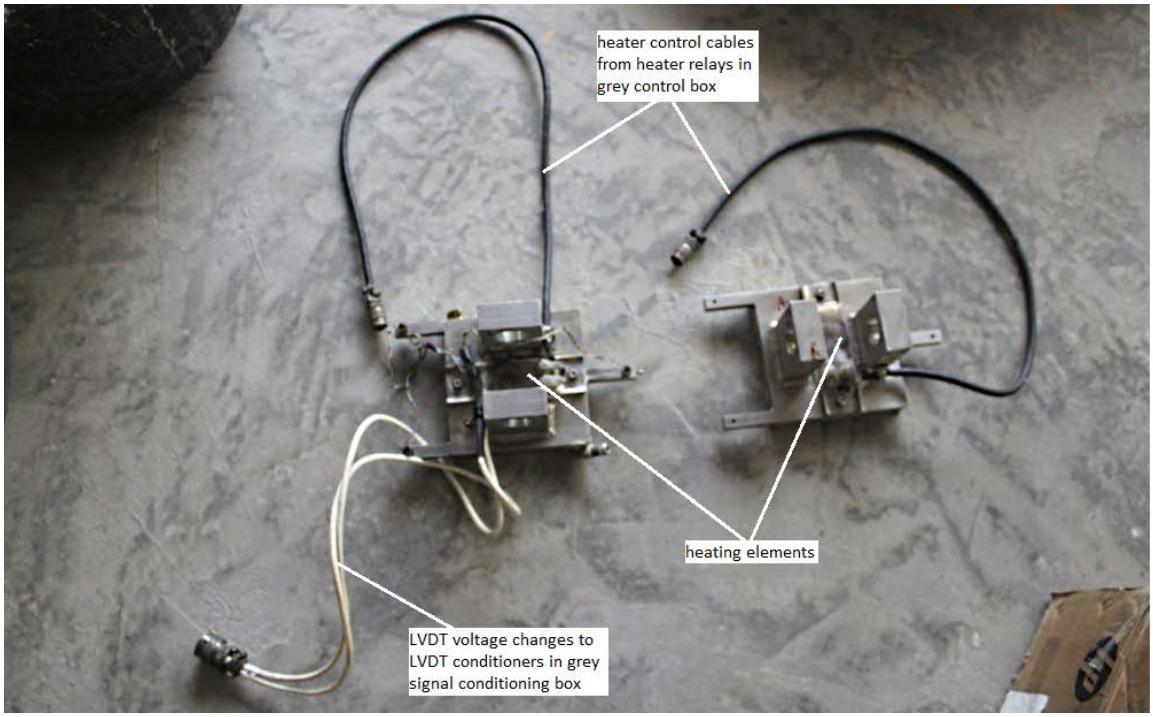

Figure 5.11 Heater system

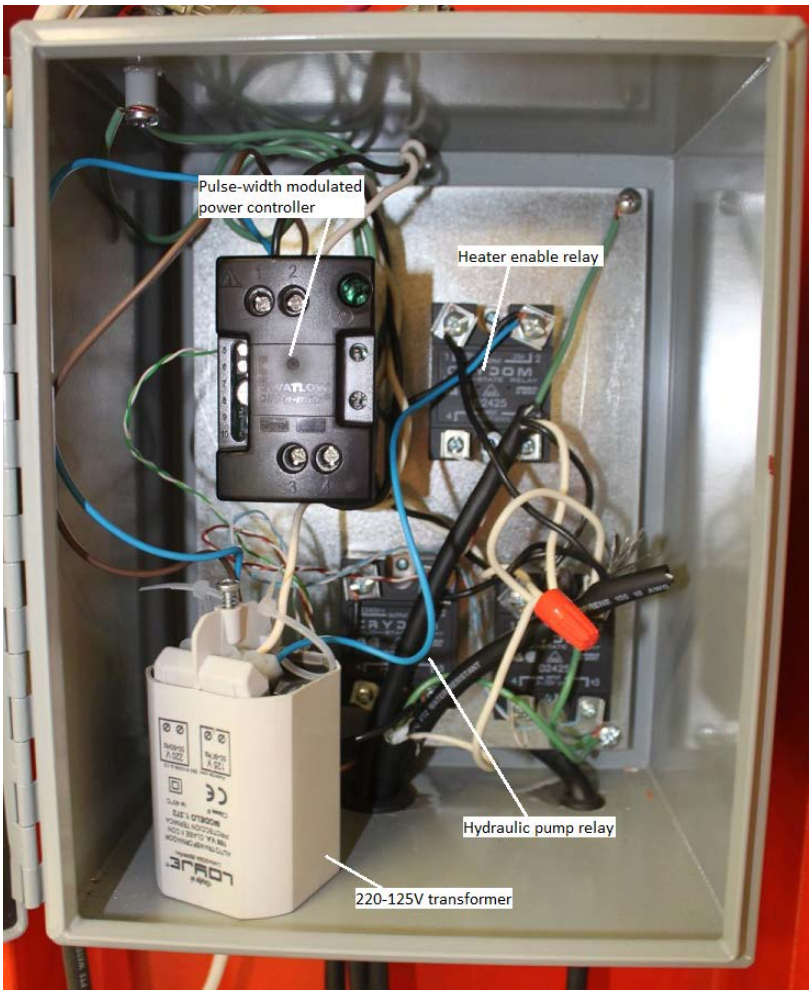

Figure 5.12 Grey heater control enclosure

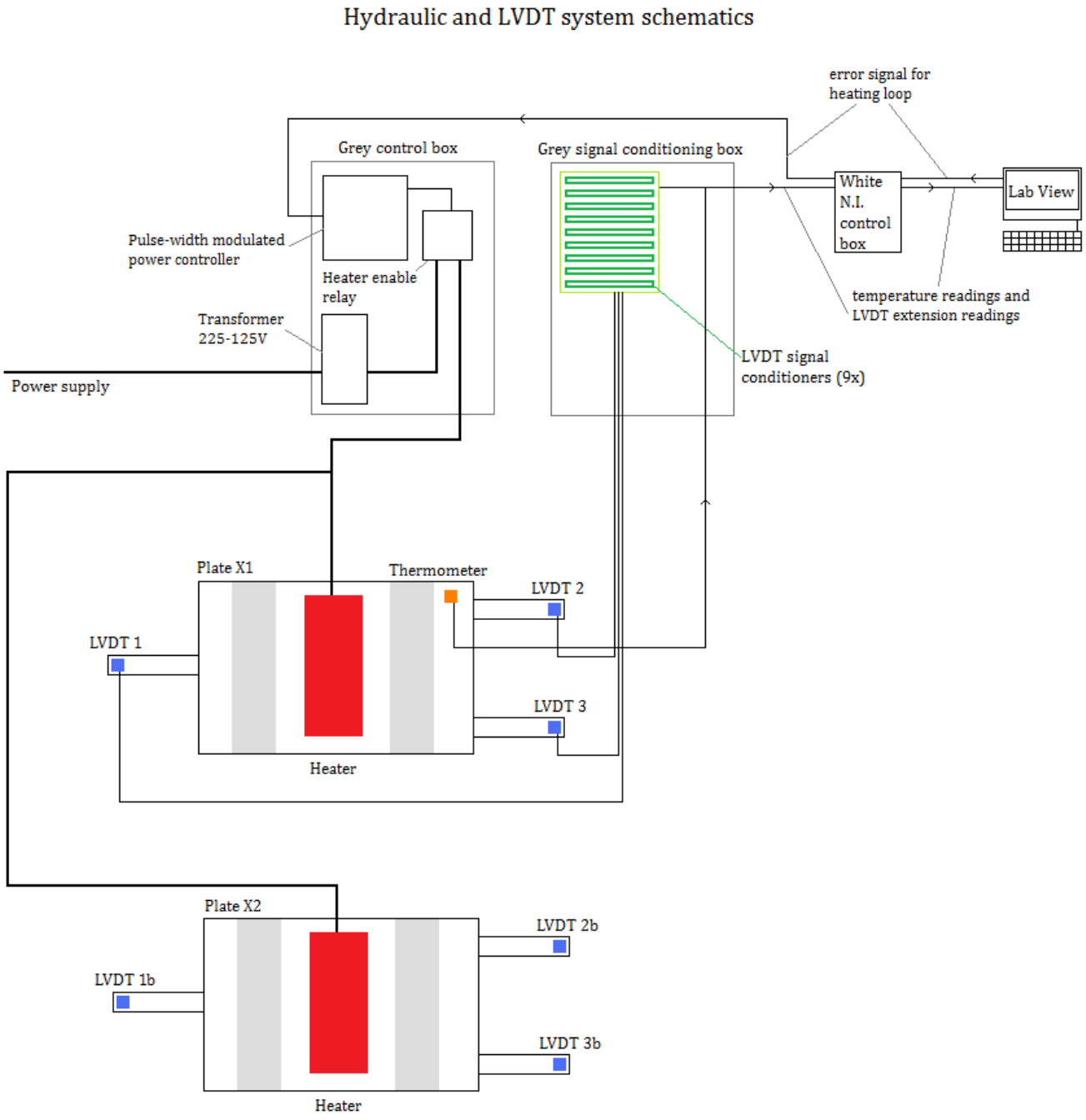

Figure 5.13 Heating and LVDT system schematics

Figure 5.13 is a schematic which shows the functioning of the heating and LVDT displacement measurement systems, as well as the flow of data to the connected PC.

5.7 Delivery of the fluid with high alkali content

The fluid system as of yet has not been set up. Upon arrival at UPC, there was no sign of any fluid delivery system, except for two holes in either side of each loading plate where the solution is obviously pumped. To keep the solution under pressure and the alkaline solution at a constant concentration, a pump will need to be installed to maintain adequate

circulation of the solution. In addition, a mixer will need to be installed in the main reservoir of fluid to ensure the concentration of alkalis stays constant, and also a heater will need to be installed to keep the solution at the same temperature as the concrete specimen. Figure 5.14 shows a loading plate, with the space for fluid circulation and the entrance and exit holes.

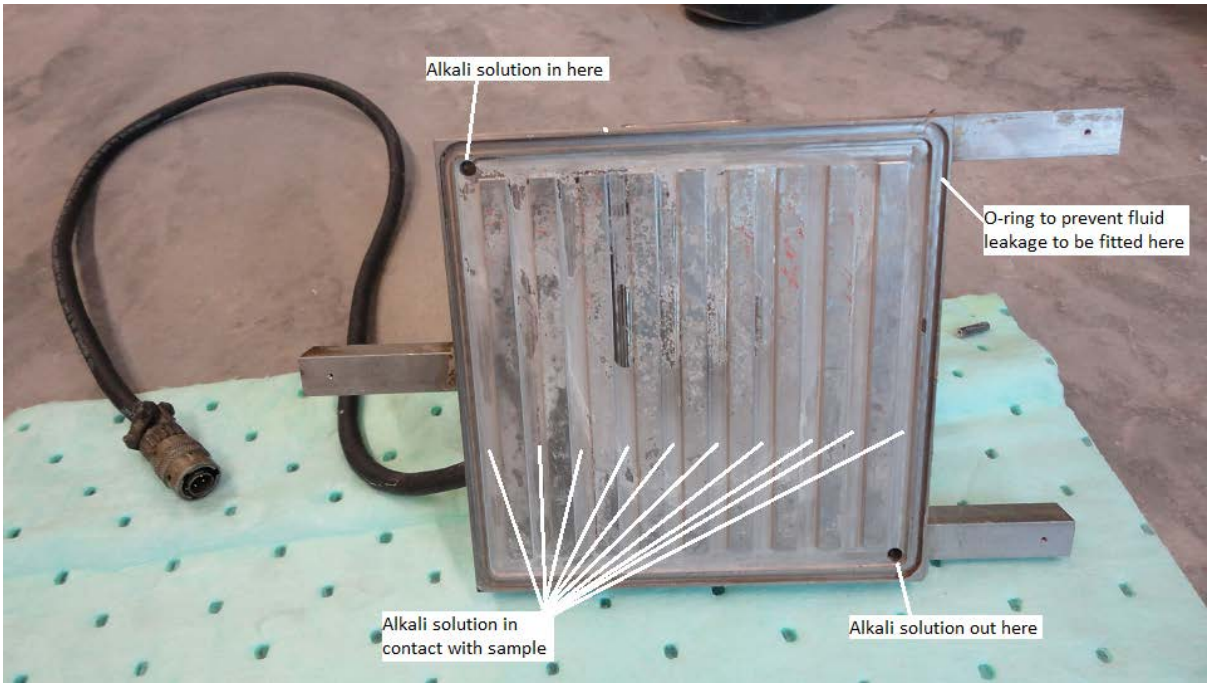

Figure 5.14 Alkali fluid delivery system

5.8 Control using LabVIEW software

LabVIEW is a program written for the control of real life systems through a visual user interface. The program simulates the functioning of real life objects known as Virtual Instruments (VI's). This means that it is not necessary to write a source code - instead the user manages a set of VI's that together represent the real processes that are occurring and being monitored by the program.

The LabVIEW VI named AARmain.vi is the top level program that controls the system.

A PC with a National Instruments PCI 6229 analog 16-bit data acquisition card receives all data from the sensors – temperature, expansion, and pressure values. This data is down sampled by the acquisition card to 1000Hz, and then in LabVIEW 2010 it is again down sampled to 10Hz, which is the refresh rate of all values on the front panel view. The LabVIEW control program also produces the temperature error signal used to control the heater, and controls the bursts of air that increase the pressure in the hydraulic pumps.

Within the program, there are two subroutines which control the two closed loop systems. One routine controls the heater system with a proportional controller (0-100%), while the

other controls the hydraulic pump which is either set to the on or off state (either allowing in air to the hydraulic pump, or not).

There are two different ways to view the program, the front panel view and the block diagram view.

5.8.1 Front panel view

The front panel is the GUI which displays useful information being collected on the progress of the reaction, and is the interface through which important conditions of the reaction are controlled. This is shown in Figure 5.15.

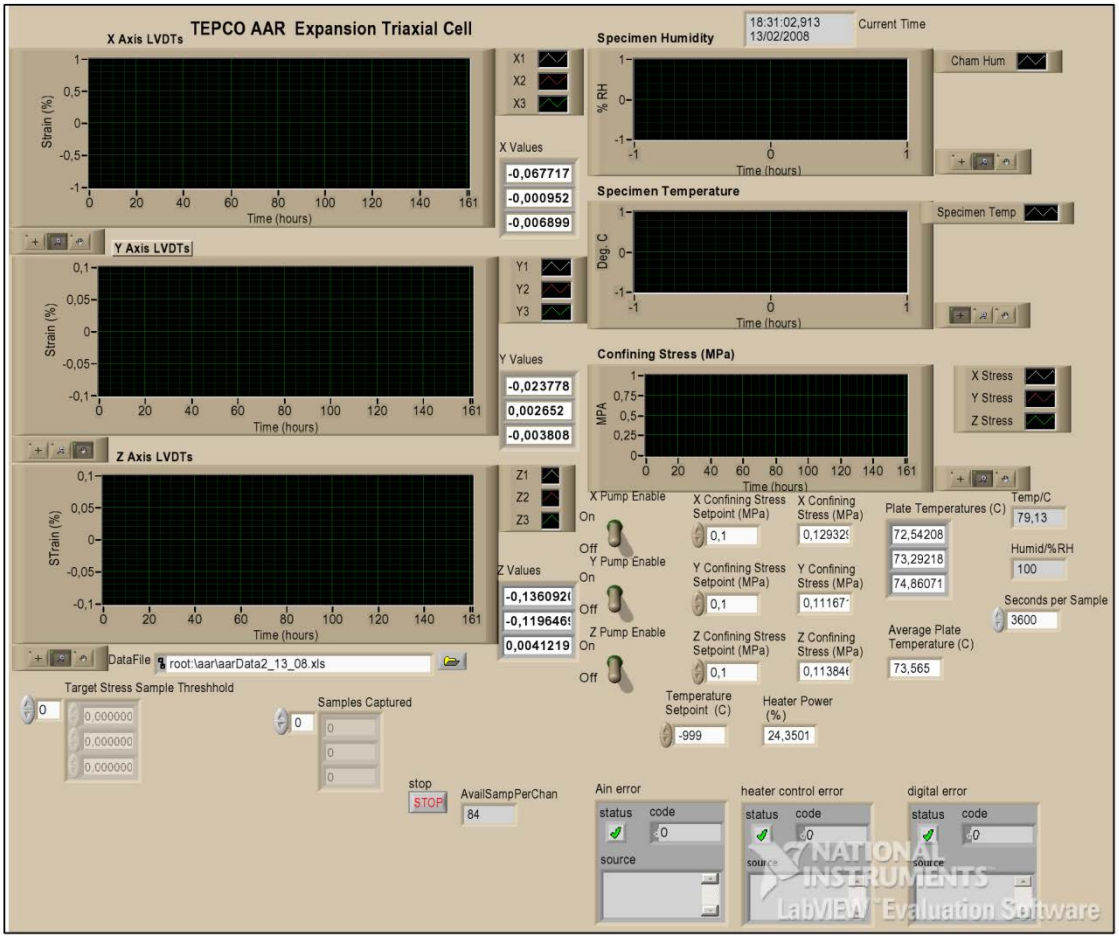

Figure 5.15 LabVIEW front panel view

In this view, there are three important input fields which act as the controls for the reaction:
1) The activation of the pumps to allow the computer to increase pressure in each axis.
2) The required confinement stress for each axis.
3) The required specimen temperature.

This view provides important information, with a refresh rate of 10Hz, on the deformation of the sample in each direction, the temperature of each loading plate (and the average), and any errors the program may have encountered.

5.8.2 Block Diagram view

This view shows exactly what is happening within the program, showing every VI and subroutine which controls the real-life apparatus and collects data from it. The left portion of the screen-shot (Figure 5.16) shows the configuration of the real hardware, and the right side is the main loop portion of the control program.

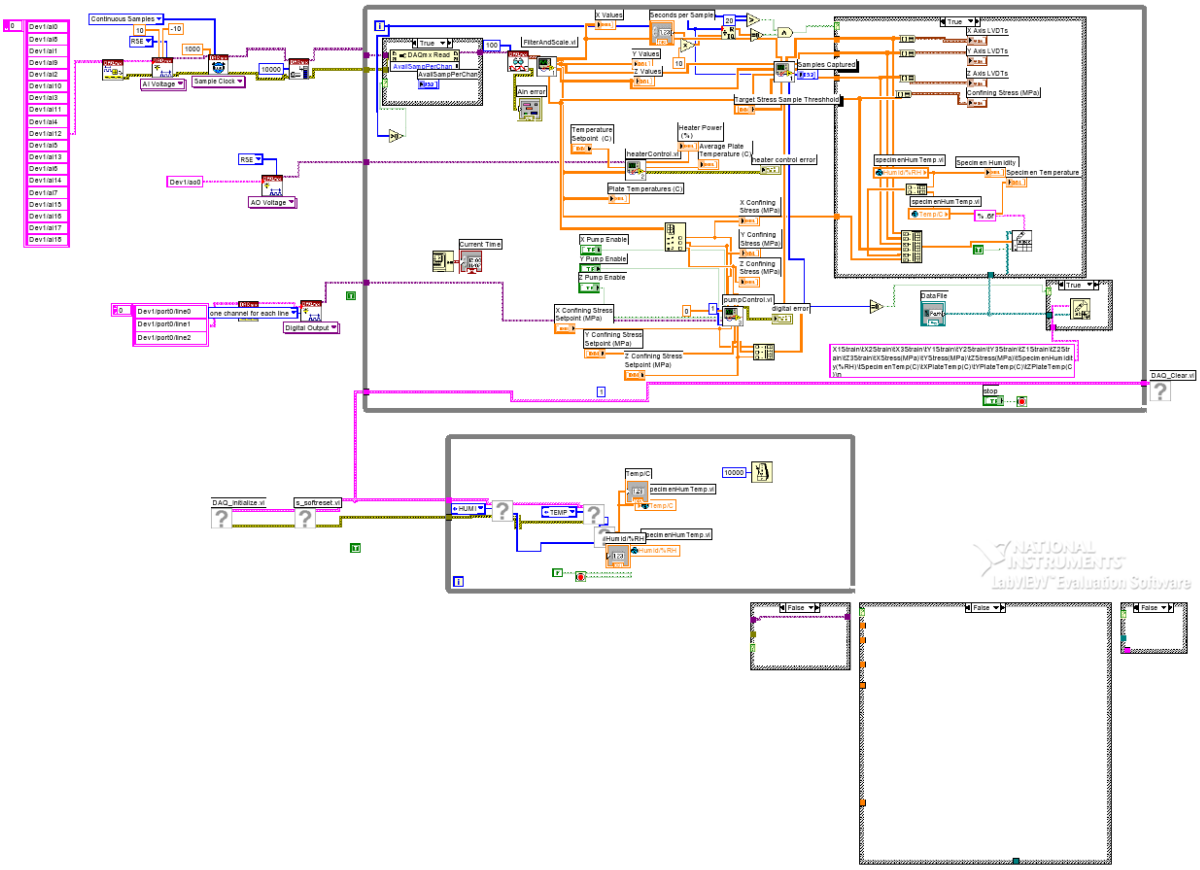

Figure 5.16 LabVIEW Block Diagram

5.8.3 Installation of LabVIEW

The applications installation was straight forward, with drivers being obtained from the National Instruments website for the PCI data acquisition card. The LabVIEW 2010 Installation CD is with the computer in the laboratory and the drivers were downloaded in a large “NIDAQ930f2” installation file still on the laboratory PC.

5.9 Operation of the machine

To run the machine, a set order must be followed. The steps for this are the following: (Saouma & Wallen, 2007).

1. Verify the electrical and compressed air supplies.
2. Remove the three active loading plates, taking care that all sensor connectors to them have been disconnected.

3. Insert the concrete specimen, and align it with the three passive loading plates.
4. Reinstall the three active loading plates, in the order X, Y and finally Z.
5. Connect each power and signal cable to its corresponding connector on the loading plates.
6. Carefully activate the hydraulic pump to drive the hydraulic actuator, with small bursts, and wiggle the loading plate as it comes into contact with the specimen, to ensure that when it starts to apply load it is flush with the specimen. The loading plates should be square with and centred on the specimen corners.
7. Remove the extension rods (with the LVDT cores screwed into their ends) from their protective containers and install them in the appropriate locations in the loading plates. These assemblies are fragile, so utmost care needs to be taken.
8. On the LabVIEW control program, set the desired confining stress and enable the hydraulic pump.
9. Manually, adjust the pressure relief valve. This is necessary because using bursts of compressed air can overshoot the pressure required, and the system is incapable of lowering the pressure automatically – this needs to be done manually.
10. Fine tune the pressure relief valve to achieve a 10-20 minute cycle time on the hydraulic pump.
11. Set the desired temperature in LabVIEW – it will take about an hour for the specimen's temperature to stabilise at this value.
12. Carefully screw each extension rod into or out of its attachment point to zero the strain reading.

Comments from a document prepared by (Polkinghorne, 2009) on the running of the machine in Colorado noted that:

- If the gray heater control box is plugged in then the temperature setpoint must be low enough to avoid the heating elements turning on. If the heater elements are on too long then this could melt the wiring.
- Any solution being pumped through the specimen should be kept from leaking onto the wiring as prolonged exposure can damage and corrode.
- Care must be taken when using the hydraulic pump to apply the pressure plates to the sample, as they must apply the load square and not at an angle.

These comments have been included as they give a good background as to the day to day operation of the machine, a stage which during this year was not reached but will undoubtedly be relevant in the year to come.

6. Conclusion

6.1 Current status of machine and potential issues

Due to the changes made during assembly of the machine and setup, there are several issues which could potentially affect the accuracy of results and the overall running of the machine. Before tests are carried out, it would be prudent to run some basic tests for which solutions are known, to verify the accuracy and find any potential issues.

Having bled the hydraulic system, it should be free from air bubbles. However, there is always the likelihood of them having entered during hose connection and so this should be kept in mind during first pressurisation of the system. Air bubbles would damage the interior lining of the hoses, and would affect linear the pressurisation of the system, therefore could interfere with the accurate ramping up of pressure during application of load.

The alkali solution delivery system has not been installed, nor were any components of this system sent to UPC with the machine. This system will need to include a central reservoir, from which the solution will be pumped around. In addition to a pump, this setup will require a heater to maintain the solution at the same temperature as the specimen, and a mixer to keep the concentration of alkalis uniform.

The computer connected to the machine is capable of opening the main LabVIEW program and the control VI, however it is not new and tends to hang. Installation of LabVIEW required several attempts as the computer would stop responding. The running of the control VI should theoretically not use much processing power and the current computer should be able to run this; however subsequent use may indicate an upgrade is necessary.

The manufactured brass LVDT extensions should theoretically work 100% as accurately as the original ones from Colorado; nevertheless it would be recommendable to use the original ones. The main reason for this is the slight increase in thickness of the brass ones. They move freely within the LVDT; however when the machine is set up they are more likely to rub against the LVDTs than the original extensions and so this could introduce error.

6.2 Final Comments

The aim of the work carried out this year was the assembly of the AAR tri-axial machine in preparation for use. There have been several obstacles to this, but now at the end of the year the machine is close to being able to run its first test. Assembly of the machine has been slow and many small setbacks have been encountered, all of which have not been detailed in this thesis. This thesis has analysed the reasons for the design and construction of the machine in the first place, and it has explained in detail the functioning of the machine so that the next people to use the machine will have a record of the work carried out this year.

The next steps in the preparation of the machine for use will be the pressure testing of the hydraulic system. This has already been filled with oil in preparation for use and should be ready for use. A pressure test will reveal any weak points of leaks in the system, should there be any. The LabVIEW computer software is loaded on the laboratory PC with the necessary drivers and the control program AARmain.vi is also loaded, so that is ready for operation. The extensions and LVDT cores are ready for use, and the cables are labelled and ready to be connected, so in terms of setting up the machine is ready to go.

The machine will be able to contribute substantially to research in the field of alkali-silica reactions, as it is uniquely placed as a one off machine capable of subjecting the alkali-silica reaction to anisotropic loading. This will contribute to ongoing work at UPC to develop a true, multi-scale (micro, meso and macro) functioning model of the ASR by providing experimental results useful for calibration of model constants and checking model predictions match experimental results.

7. Bibliography

Bournazel, J. P., & Moranville, M. (1997). *Durability of Concrete*: *The crossroad between chemistry and mechanics.*

Brehm, D. (2009). *MIT engineers find way to slow concrete creep to a crawl*. Retrieved 06 10, 2011, from MIT: http://web.mit.edu/newsoffice/2009/creep-0615.html

Canadian Strategic Highway Research Program. (1996). *Alkali-Silica Reactivity.* Transportation Association of Canada.

Comby-Peyrot et al. (2009*). Development and validation of a 3D computational tool to describe concrete behaviour at mesoscale, application to the Alkali-Silica Reaction.* Computational Materials Science .

Dent-Glasser, L. S., & Kataoka, N. (1981*). The chemistry of alkali-aggregate*. Proceedings of the Fifth International conference on Alkali-Aggregate, (p. 66).

Erik Schlangen, O. Ç. (2007). *Modelling of effect of ASR on concrete microstructure.*

Farny, J., & Kerkhoff, B. (2007). *Diagnosis and Control of Alkali-Aggregate Reactions in Concrete.*

Glasser, F. P. (1992). *Chemistry of the alkaliaggregate.* Blackie and Son Ltd.

Hooton, R., & Rogers, C. (1988). *Evaluation of rapid test methods for detecting alkali-reactive aggregates.* Proceedings of the Eighth International Conference on Alkali-Aggregate reaction (pp. 439-444).

Jones, A. E., & Clark, L. A. (1998). *The effects of ASR on the properties of concrete and the implications for assessment.* Elsevier Ltd.

Larive, C. (1998). *Combined contribution of experiments and modelling to the understanding of alkali-aggregate reaction and its mechanical consequences .*

Léger et al. (1997). *Finite Element Analysis of Concrete Swelling Due to Alkali-Aggregate Reactions in Dams.* Canadian Society for Civil Engineering - Annual Conference, (pp. 620-630).

López et al. (2011). *Problemática de las reacciones expansivas en presas.*

Martinez, D. M. (2010). Analisis de la aplicabilidad de arenas de dragado marino como arido fino en morteros y hormigones. (pp26).

Multon et al. (2003). *Structural Behavior of Concrete Beams Affected by Alkali-Silica Reaction*. ACI Materials Journal , (pp67-76).

Rogers, C. (1990). *Interlaboratory study of the concrete prism expansion test for the alkalicarbonate*. Canadian Developments in Testing Concrete Aggregates. (pp136-149).

Saouma, V., & Perotti, L. (2006). Constitutive *Model for Alkali-Aggregate Reactions.* ACI Materials Journal, (pp194-202).

Saouma, V., & Wallen, R. (2007). *Triaxial Cell for the Heated Expansion of AAR Specimens.* Tokyo Electric Power Service Company.

Saouma, V., & Xi, Y. (2004). *State of the Art Survey of Alkali-Aggregate Reactions in Dams.*

Schlangen, E., & Çopuroğlu, O. (2007). *Modelling of effect of ASR on concrete microstructure.*

Suwito, A., W.Jin, Xi, Y., & Meyer, C. (2002). *A Mathematical Model for the Pessimum Size Effect of ASR in Concrete.*

Swamy, R. (2009). *Testing for alkali-silica reaction.*

Winter, N. (2001). *Alkali-Silica reaction in Concrete*. Retrieved 06 18, 2011, from Understanding Cement: http://www.understanding-cement.com/alkali-silica.html

Winter, N. (2005). *Hydration*. Retrieved June 17, 2011, from Understanding Cement: http://www.understanding-cement.com/hydration.html

Polkinghorne, K. (2009). *Readme (sent with documentation on AAR tri-axial machine).*

(Author not stated) *Cement.org*. (2011). Retrieved 2011, from http://www.cement.org/tech/faq_asr.asp

Hydroxylation. (2011, 01 12). Retrieved 07 15, 2011, from Wikipedia: http://en.wikipedia.org/wiki/Hydroxylation

Civil Engineering Portal. (2011). Retrieved 06 10, 2011, from Modulus of Elasticity of Concrete: http://www.engineeringcivil.com/modulus-of-elasticity-of-concrete.html

Macro Sensors. (2003). *LVDT Basics.* Retrieved 06 20, 2011, from Macro Sensors: http://www.macrosensors.com/lvdt_tutorial.html

Mishra, G. (2010). *The Constructor - Civil Engineering home*. Retrieved 07 11, 2011, from http://theconstructor.org/concrete/alkali-aggregate-reaction-in-concrete/67/